Spring 2019

# Landslide Detection Using Remote Sensing Methods A Review of Current Techniques

Sumanth Varma Byrraju

Recommended Citation

Byrraju, S. V.(2019). *Landslide Detection Using Remote Sensing Methods A Review of Current Techniques.* (Master's thesis). Retrieved from https://scholarcommons.sc.edu/etd/5105

# LANDSLIDE DETECTION USING REMOTE SENSING METHODS A REVIEW OF CURRENT TECHNIQUES

by

Sumanth Varma Byrraju

Bachelor of Engineering
Vasavi college of Engineering, 2012

---

Submitted in Partial Fulfillment of the Requirements

For the Degree of Master of Science in

Civil Engineering

College of Engineering and Computing

University of South Carolina

2019

Accepted by:

Dimitris Rizos, Director of Thesis

Robert L Mullen, Reader

Juan Caicedo, Reader

Cheryl L. Addy, Vice Provost and Dean of the Graduate School

# Abstract

Landslides are among the most dangerous natural disasters, as they generally follow other major disasters thereby causing significant damage to already weakened systems.  In the U.S. alone they cause an excess of 1 billion in damages and an average 25-50 deaths annually(USGC). Remote sensing techniques for landslide monitoring and prediction has gained popularity in recent years since it enables hazard mitigation. Synthetic Aperture Radar (SAR) interferometry is among the remote sensing techniques used.  DInSAR is an advanced interferometric technique which uses radar sensors to estimate the phase of a given area from which the landslide activity can be predicted. The analysis has been performed in 3 test areas each having unique conditions. These areas have been chosen to assess the effectiveness of the analysis in their respective conditions.

The data for this analysis is obtained using Sentinel-1 satellite which is a C-band SAR sensor. The 3 locations have been analyzed for a period of 36 days with sensor taking acquisitions every 12 days. From this analysis, we have found in the case of Etna slope instability due to volcanic action has been observed. In the case of California highway-1 a unique phase activity was observed in the landslide region which suggest additional analysis to be performed in similar conditions to validate the findings. Finally, in the case of Anargyroi Greece bad phase readings in the region resulted in uncertain analysis prompting for longer time series analysis to mitigate these problems.

Additional subsidence maps were also generated from the phase, but these results could not be calibrated and correlated with in situ readings. To assess the effectiveness of this method to quantify subsidence monitoring additional analysis must be done which take in to consideration old phase values for accurate results.

# Table of Contents

Abstract ... iii

List of Figures ... viii

Chapter 1 Introduction to Landslides ... 1

- Historic importance ... 1
- Landslide Description ... 2
- Landslide Classification ... 6
- Causes of Landslide ... 11
- Traditional Method for Landslide Investigation ... 12

Chapter 2 Brief Introduction to Remote Sensing ... 14

- Electromagnetic Spectrum ... 14
- Sensor ... 16

Chapter 3 Landslide Investigation Using Remote Sensing ... 19

- Landslide Recognition ... 19
- Landslide Monitoring ... 32

Chapter 4 Using InSAR for Landslide Recognition ... 42

- Introduction to InSAR ... 42
- InSAR Methodology ... 43

  SAR ..... 48
  InSAR ..... 49
  DInSAR ..... 52
Chapter 5 DInSAR Implementation ..... 56
  Step-1 Coregistration ..... 58
  Step-2 Interferometric Process ..... 58
  Step-3 Deburst ..... 59
  Step-4 Merge ..... 59
  Step-5 Topographic Phase Removal ..... 59
  Step-6 Phase Filtering ..... 60
  Step-7 Phase Unwrapping ..... 60
  Step-8 Displacement Analysis ..... 60
  Step-9 Terrain Correction ..... 61
Chapter 6 DInSAR Showcase Studies ..... 62
  Satellite Information ..... 62
  Study Areas Description ..... 62
  Datasets ..... 64
  DInSAR Application in ETNA ..... 66
Chapter 7 Results and Discussion ..... 71
  Mount Etna ..... 71

Discussion ........................................................................................................ 76

California Highway-1 ............................................................................................ 77

Discussion ........................................................................................................ 81

Anargyroi Greece ............................................................................................ 82

Discussion ........................................................................................................ 88

Chapter 8 Conclusions and Recommendations ....................................................89

Conclusion ........................................................................................................ 89

Recommendations ............................................................................................ 89

PInSAR ............................................................................................................ 90

Application of InSAR in Railway ........................................................................ 90

References ..............................................................................................................92

APPENDIX A List of Definitions .............................................................................98

# List of Figures

Figure 1.1: Iconic image in Kedarnath before and during landslide (Hindustan Times, 2013) ........1

Figure 1.2: Different Parts of a landslide as per IAEG (The Canadian Geotechnical Society, 1993) ........4

Figure 1.3: Example of different type of landslide movements (H.Cornforth, 2005). ........9

Figure 2.1: This picture represents the Electromagnetic (EM) Spectrum ........14

Figure 2.2: This image describes how different wavelengths of E.M. spectrum behave with water, oxygen and ozone. These **c**omponents constitute most of the atmosphere (Pamela, 2009**)**. ........16

Figure 3.1: In image A, combination of visual interpretation and automatic pixel recognition methods are used to detect landslides. Images B and C show the landslide detected using the above method. Image B shows the location before the event and image C shows the landslide after the event(Lacroix et al. 2013). ........21

Figure 3.2: Images of landslides recognized by color ortho-photographs (A and B) and panchromatic images (C and D). The yellow lines highlight the detected landslide. (Fiorucci et al. 2011) ........22

Figure 3.3 : In this image landslide were detected using IHS image fusion technique. (Marcelino, Formaggio, and Maeda 2009) ........23

Figure 3.4: The above image (A) shows the detected landslides and the corresponding pan-sharpened fusion image (B) (Wong, 2005) ........24

Figure 3.5: The image (A) represents the stereo image used to detect landslides. The landslides detected using image A are shown image B (Alkevli and Ercanoglu 2011) ....25

Figure 3.6: Image A shows the stereo mirror system to view stereo image. Image B shows the landslide DEM from GeoEye-1 stereo pair (Murillo-García et al. 2015)........26

Figure 3.7: Deep seated landslides are detected from eigenvalue and slope filter ratio obtained from airborne LIDAR. The image above represents the spatial distribution of slope angle (Kasai et al. 2009) ........27

Figure 3.8: Image A shows the moving average filter map for slope and landslide. Image B shows the average correlation texture map for DTM and landslide locations. landslides in both images are marked by dotted line (Chen et al. 2014) ..........................................28

Figure 3.9: As the key indicates the above image represents the landslides detected from semi-automatic landslide methods along with some false positives (Moine, Puissant, and Malet 2009)..........................................................................................................29

Figure 3.10: image A shows the final result of the landslides detected using the automatic method marked in yellow. image B shows the false positive obtained from this method marked in green (Lu et al. 2011)..........................................................................30

Figure 3.11: The above images represents the fringe pattern from InSAR .2 pass processing in A, 3 pass processing in B and enlarged image representing movement rates around 14mm in 3 months (A.Walther, 2008)..................................................................31

Figure 3.12: The above images represent the landslides detected from (A) C-band satellite and (B) L-band satellite. The arrow indicates the unstable area which is visible in both the images (Delacourt et al. 2009)................................................................32

Figure 3.13: Displacement map obtained by correlation between aerial photographs. A is the displacement map between 1999 and 2003 and B is the displacement map between 1995 and 1999. NC from the scale represents no significant displacement because of poor correlation values(C. Delacourt et al. 2004)......................................................34

Figure 3.14 DEMs obtained from LiDAR datasets show the landslide. The dotted line points the outline and progression of landslide in years A (2005), B (2006), C (2007)(Corsini, A and Cervi, F and Daehne, A and Ronchetti 2009) ...............................36

Figure 3.15: (A) represents the ground motion activity detected by PSI. (B)Landslide inventory map updated in Tramuntana Range with (C) representing the statistical evaluation of landslide database improvement (Bianchini et al. 2013)............................37

Figure 3.16: (A)represents the field set up of instrumentation (B) shows the technical scheme the equipment (C)shows the DEM of the target scene projected represented in local coordinate system with center being the point of origin (Tarchi et al. 2003) ..........39

Figure 4.1: This is the reference scale for the E.M spectrum based on wavelength of light ..........................................................................................................44

Figure 4.2: This image shows the working of an active radar sensor which illuminates its target with its own energy.......................................................................................44

Figure 4.3: The figure shows the radar imaging geometry...............................................45

Figure 4.4: Successive ranging pulses are transmitted synchronously with platform velocity to cover most of the terrain ....................................................................44

Figure 4.5: Simplified diagram of the radar receiver. Which shows the creation of real and imaginary part of the image from which the phase and amplitude are developed......47

Figure 4.6: This image shows a chart of present and past SAR satellites .........................54

Figure 4.7: This image shows the microwave penetration of different SAR sensors........55

Figure 5.1: This image shows the flowchart followed for DInSAR analysis ....................57

Figure 6.1: This image shows the significance of each part of the sentinel-1 dataset.......64

Figure 6.2: Image A was taken on 14 march and image B was taken on 26th March.......66

Figure 6.3: image shows a typical interferogram before any filtering is done, the Demarcation zones are visible ..........................................................................................67

Figure 6.4: The image shows an interferogram in which the demarcation zones are removed...........................................................................................................................67

Figure 6.5: The image shows the interferogram after merging 2 subsets..........................68

Figure 6.6: In This image, the topographic phase has been removed, although the displacement phase is visible significant noise is still available.......................................68

Figure 6.7: In this image, the displacement phase is clearly visible and are highlighted.....................................................................................................................69

Figure 6.8: The image shows the displacement in the direction of satellite line of sight .......................................................................................................................69

Figure 6.9: In this image, the displacement map is super imposed on google earth file for better understanding of the displacement ..........................................................................70

Figure 7.1: This is Mount Etna observed through the visual spectrum. This image shows the target area to be analyzed...........................................................................................71

Figure 7.2: The image describes the phase properties of Mount Etna and does not have any significant phase variations which signify slope instability.......................................72

Figure 7.3: The black region in the center describes the low signal strength and the whitish grey surrounding signifies high signal to noise ratio signifying better phase reading in this region .......................................................................................................72

Figure 7.4: The above image shows minor subsidence around the image center although this reading can be considered calibration error ...............................................................73

Figure 7.5: This image does not show any significant phase variation that confirm slope instabilities in the region...................................................................................................73

Figure 7.6: The black region in the center describes the low signal strength and the whitish grey surrounding signifies high signal to noise ratio signifying better phase reading in this region ........................................................................................74

Figure 7.7: The constant subsidence visible in the image is not considered as this reading can be due to calibration error or due to minor vegetation ...............................................74

Figure 7.8: The high lightened region signifies slope instability and possible landslide activity..................................................................................................................75

Figure 7.9: Shows the coherence map of the region and from the map we can see that the center of the mount has poor coherence(black) because of this the poor coherence part is not considered for our discussion ......................................................................75

Figure 7.10: The image shows minimum displacement activity due to the volcanic action ...........................................................................................76

Figure 7.11: This image was taken before the landslide occurred by Landsat satellite.....78

Figure 7.12: This image shows effect of landslide on the highway and is taken by Landsat satellite ...............................................................................................................78

Figure 7.13: the highlighted part shows some phase disturbance which are not related to slope movement as phase corresponding to slope movement has distinct contour like pattern .................................................................................................................79

Figure 7.14: The image shows good coherence with more grey and white area signifying good signal strength .........................................................................................79

Figure 7.15: The image shows good phase reading that is visible with the location where the landslide is to take place having some activity ..........................................................80

Figure 7.16: This image shows there is high white color presence which signifies good signal to noise ratio ........................................................................................80

Figure 7.17: The landslide incident is clearly seen in the phase image with the flow covering the target region ..................................................................................81

Figure 7.18: The image shows poor signal to noise ratio in the area where the landslide has taken place but the area surrounding it has good signal to noise ratio ........................81

Figure 7.19: The above image shows the lignite mine operational and before the landslide event.................................................................................................................82

Figure 7.20: The above image shows the area after the collapse of the mine due to landslide ..............................................................................................................83

Figure 7.21: most of the image shows low phase visibility ...............................................83

Figure 7.22: From the image, we can see that only a portion of the image has good signal to noise ratio .......................................................................................................84

Figure 7.23: The developed displacement map shows that most of area has significant subsidence .......................................................................................................84

Figure 7.24: Most of the image is discolored due to high noise but the highlighted part shows phase activity corresponding to landslide activity .................................................85

Figure 7.25: The highlighted area contains acceptable coherence and corresponds to landslide activity of the region ...........................................................................85

Figure 7.26: The figure shows the displacement map of the region. The Region A shows displacement corresponding to landslide activity but must be disregarded due to poor coherence in the area. Region B does not show any subsidence related to landslide activity in the region .........................................................................................86

Figure 7.27: In the figure, the highlighted landslide incident is much clear in this image .......................................................................................................86

Figure 7.28: In the figure, the highlighted area shows good coherence and corresponds to landslide activity of the region ...........................................................................87

Figure 7.29: The figure shows the displacement map of the region. Highlighted area A shows significant subsidence but cannot be attributed to the landslide because of poor phase readings. Highlighted area B also shows significant subsidence but because this area has significantly better phase value this subsidence can be attributed to landslide ...........................................................87

# Chapter 1

# Introduction to Landslides

## Historic importance

Landslides are defined as “the usually rapid downward movement of a mass of rock, earth, or artificial fill on a slope” [https://www.merriam-webster.com/dictionary/landslide]. Landslides are one of the most dangerous natural hazards because they generally follow other natural hazards and they exploit already weakened the system. This can be seen in the case of Uttarakhand, India landslide. On 14-17 June 2013, the Indian state of Uttarakhand and surrounding states experienced heavy rainfall, this caused the melting of Chorabari glacier which is at the height of 3,800 meters and overflow of Mandakini River. The melting of snow together with heavy rainfall caused floods which weakened the surrounding landmass causing the landslide. Fig 1.1 shows the image of the popular icon before and during the landslide. The damage is also increased by heavy sand mining and coastal construction (Nair 2014).

Figure 1.1: Iconic Image in Kedarnath before and during landslide (Hindustan Times, 2013)

The Centre for Research on the Epidemiology of Disaster (CRED) (EM-DAT , n.d.) reported that Asia has 206 reported cases in 2016 out of which the landslide that occurred in china in Guangxi province (30/5/2016-03/06/2016) affected 2.1 million people alone. According to United States Geological Survey (USGS) the landslide in Utah (1983) (J. M. Duncan, 1986) destroyed major railroad and highway with a total loss of 600 million dollars, and, although there have been no deaths this landslide caused a great impact on the economy of the region. The damage caused by landslides in most cases is attributed to its triggering mechanism and not the landslide itself. It is also noted that a lot of cases go unreported because of their remote location.

The great socioeconomic impact of landslides establishes a need for the development of landslide recognition, monitoring and prediction systems that will allow hazard prevention and mitigation measures. Such systems should be fast and accurate yet cost effective. Existing traditional techniques and more innovative methods are discussed in this paper.

## Landslide Description

As the formal definition of landslide suggests, the phenomenon involves movement of land over slopes that alter the geomorphic characteristics of the region. According to the International Association of Engineering Geologist (IAEG) (IAEG, 1990) based on classification by Cruden(David M Cruden and Varnes 1996) the different features of a landslide are numbered in Fig. 1.2 and the description of these features are followed

1) Crown: the practically undisplaced material still in place and adjacent to the highest parts of main scarp (2).

2) Main scarp: A steep surface on the undisturbed ground at the upper edge of the landslide, caused by movement of the displaced material (13) away from the undisturbed ground. It is the visible part of the surface of rupture (10).

3) Top: The highest point of contact between the displaced material (13) and the main scarp (2).

4) Head: The upper parts of the landslide along the contact between the displaced material and the main scarp (2).

5) Minor scarp: A steep surface on the displaced material of the landslide produced by differential movements within the displaced material.

6) Main body: The part of the displaced material of the landslide that overlies the surface of rupture (10) between the main scarp (2) and the toe of the surface of rupture (11).

7) Foot: The portion of the landslide that has moved beyond the toe of the surface of rupture (11) and overflies the original ground surface (20).

8) Tip: The point on the toe (9) farthest from the top (3) of the landslide.

9) Toe: The lower, usually curved margin of the displaced material of a landslide, it is the most distant from the main scarp (2).

10) Surface of rupture: The surface which forms (or which has formed) the lower boundary of the displaced material (13) below the original ground surface (20).

11) Toe of surface of rupture: The intersection (usually buried) between the lower part of the surface of rupture (10) of a landslide and the original ground surface (20).

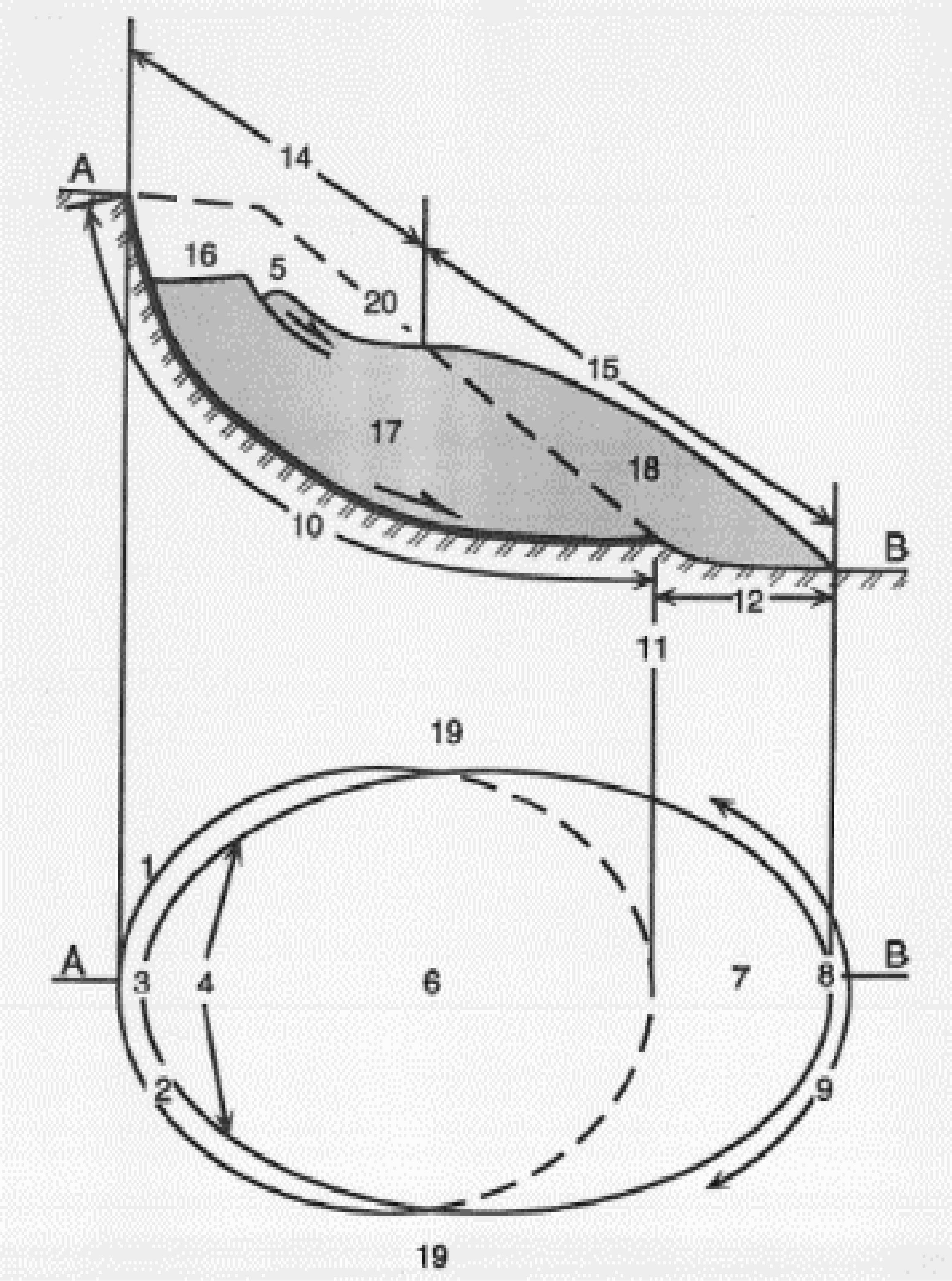

Figure 1.2: Different Parts of a landslide as per IAEG (The Canadian Geotechnical Society, 1993)

12) Surface of separation: The part of the original ground surface (20) overlain by the foot (7) of the landslide.

13) Displaced material: Material displaced from its original position on the slope by movement in the landslide. It forms both the depleted mass (17) and the accumulation (18).

14) Zone of depletion: The area of the landslide within which the displaced material lies below the original ground surface (20).

15) Zone of accumulation: The area of the landslide within which the displaced material lies above the original ground surface (20).

16) Depletion: The volume bounded by the main scarp (2), the depleted mass (17) and the original ground surface (20).

17) Depleted mass: The volume of the displaced material which overlies the rupture surface (10) but underlies the original ground surface (20).

18) Accumulation: The volume of the displaced material (13) which lies above the original ground surface (20).

19) Flank: The undisplaced material adjacent to the sides of the rupture surface. Compass directions are preferable in describing the flanks but if left and right are used, they refer to the flanks as viewed from the crown (1).

20) Original ground surface: The surface of the slope that existed before the landslide took place.

## Landslide Classification

Landslides are broadly classified in three categories based on size, velocity and failure flow.

### *Landslide based on size*

Table 1.1 explains the classification based on the size of the landslide.

Table 1.1: Grouping of landslides based on their area (D. M. Cruden et al. 1994)

| Descriptor | Area (sq.ft.) | Area (sq.m.) |
|---|---|---|
| **Very small** | <2000 | <200 |
| **Small** | 2,000-20,000 | 200-2,000 |
| **Medium** | 20,000-200,000 | 2,000-20,000 |
| **Large** | 200,000-2,000,000 | 20,000-200,000 |
| **Very large** | 2,000,000-20,000,000 | 200,000-2,000,000 |
| **Huge** | >20,000,000 | >2,000,000 |

It should be noted that the description based on size is not a standard form of description.

### *Landslide based on velocity*

Table 1.2 explains the classification based on the velocity of landslide by Cruden. The term Creep has been omited as the word has multiple definitions in different litratures. This classification is later updated by World Landslide Inventory(WLI) as mentioned.

Table 1.2: Grouping of landslides based on their velocity(David Milne Cruden 1996)

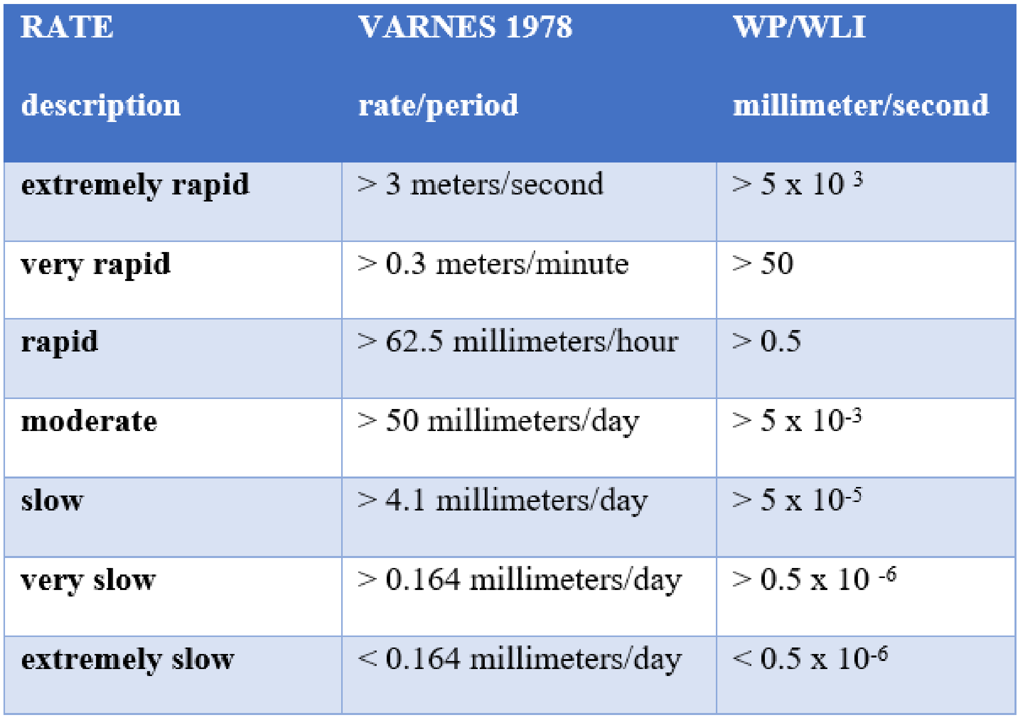

| RATE<br>description | VARNES 1978<br>rate/period | WP/WLI<br>millimeter/second |
|---|---|---|
| **extremely rapid** | > 3 meters/second | > 5 x $10^{3}$ |
| **very rapid** | > 0.3 meters/minute | > 50 |
| **rapid** | > 62.5 millimeters/hour | > 0.5 |
| **moderate** | > 50 millimeters/day | > 5 x $10^{-3}$ |
| **slow** | > 4.1 millimeters/day | > 5 x $10^{-5}$ |
| **very slow** | > 0.164 millimeters/day | > 0.5 x $10^{-6}$ |
| **extremely slow** | < 0.164 millimeters/day | < 0.5 x $10^{-6}$ |

*Landslide based on slope movement*

A better and more accurate form of classification was suggested by Varnes and Cruden (David Milne Cruden 1996) which develops landslide classification based on slope movement. This mode of classification is followed by USGS and can be considered to be a standard while describing a landslide. These are depicted in Fig 1.3 and discussed as follows.

Falls

A fall can be described as soil or rock detaching from a steep slope with little or no shear displacement prior to the occurrence. This happens very rapidly and followed by the detached material to bounce and roll. The velocity of the detached material depends on the steepness of the slope. They are common worldwide, generally occur on steep and vertical slopes, but also near coastal areas, along rocky banks of rivers and streams. In the fig (1.3) they are represented by letter D.

### Topples

When a mass of soil or rock rotates forward around a point below the center of gravity it is considered a topple. Topples are common in columnar-jointed volcanic terrain and near rivers where the banks are steep. Their speed varies and sometimes the mass accelerates along the slope depending on the distance of travel. In the fig (1.3) they are represented by letter E.

### Slides

These are downward movement of mass occurring on the surface of failure or on thin zones of intense shear strain. The volume of mass enlarges from an area of local failure. They are divided into 2 types.

### Rotational

This occurs when the surface of failure is “spoon-shaped” and the mass moves downward and outward on the concave surface. They occur in homogeneous “fill “materials. In the fig (1.3) they are represented by letter A.

### Translational

This type of slides occurs when the mass moves out and down along a planar surface as compared to rotational slides with minimal rotational movement. Unlike rotational slides which tend to restore equilibrium, translational slides progress over considerable distance if the surface is inclined. Translational slide failure occurs along faults and joints. In the fig (1.3) they are represented by letter B.

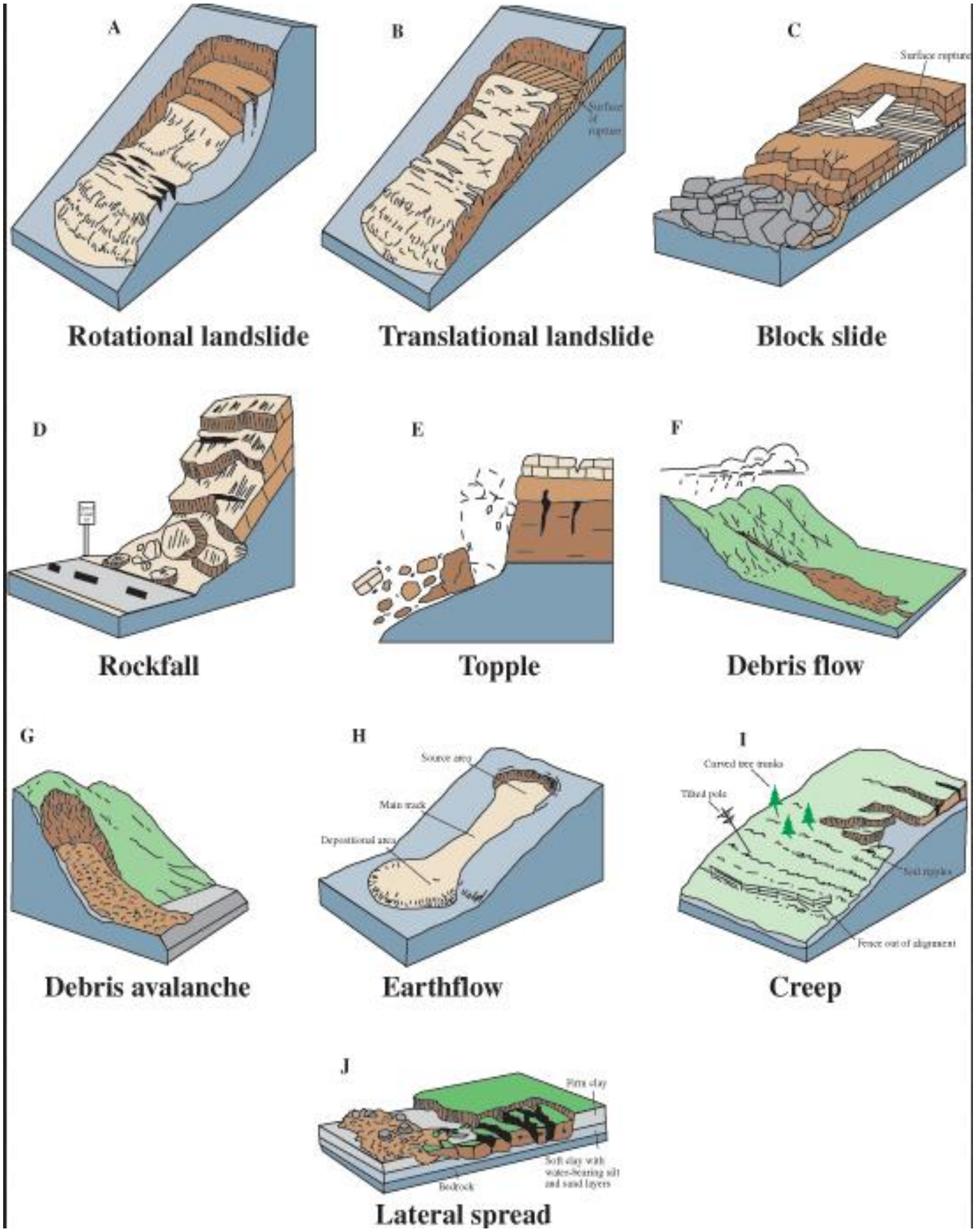

Figure 1.3: Example of different type of landslide movements (H.Cornforth, 2005).

Lateral spreads

These are unique to other landslides as they occur on flat or gentle slopes. This type of failure occurs when the failure surface is hard as compared to the layer below it.

The failure surface breaks away slowly and in some cases, remains intact. These are generally the result when liquefaction of subsurface occurs followed by triggering events like earthquake/shaking. In the fig (1.3) they are represented by letter J.

### Flows

The failure mass resembles a vicious liquid. This is because of actions from heavy rainfall affecting weak slopes which together form a slurry-like material which flows. These are further divided into.

### Debris flow

This type of landslides occurs when loose soil, rock, and organic matter combine with water from either rain or snowfall to form a slurry that flows downslope. These are also called mudslides this is a misinterpretation due to large quantities of fine material in the slurry. Sometimes if translational slide and rotational slides gain velocity they evolve into debris flow as the internal mass loses cohesion. In the fig (1.3) they are represented by letter F.

### Debris avalanche

Debris avalanche is essentially debris flow which is large and extremely rapid. These are further divided into cold and hot types based on triggering mechanisms. If the avalanche is caused by volcanic action it is considered hot type like an injection of magma causing instability. A cold type of debris avalanche occurs when the slope becomes unstable from weathering action. In the fig (1.3) they are represented by letter G.

### Creep

This is a form of earthflow which is slow and steady. This is caused by internal shear stress sufficient to cause deformation but insufficient to cause failure. This is one of the most common type of landslide and additional triggering effects will make it rapid and more damaging type. In the fig (1.3) they are represented by letter I.

### Earth flow

This occurs when the susceptible quick clay is disturbed causing it to lose its shear strength and suddenly liquefy. This can happen due to saturation of soil due to intense rainfall or excessive loading on the slope or other natural reasons like earthquake. This mass in earthflow moves as viscous flow with large internal deformations. In the fig (1.3) they are represented by letter H.

## Causes of landslide

The main causes of landslides are geological, morphological and human. Geological causes include weathered, sheared, jointed or fissured materials, adversely orientated discontinuities, permeability and material contrasts, rainfall and snowfall and earthquakes. Examples of Morphological causes include slope angle, uplift, rebound, erosion (fluvial, wave, glacial or subterranean), erosion of lateral margins, slope loading and vegetation change. Human factors pertain to deforestation, excavation, loading, water management (groundwater drawdown and water leakage), land use (e.g. construction), mining and quarrying, vibration and pollution among others.

## Traditional method for landslide investigation

Traditional landslide investigation refers to methods which do not consider or use any form of remote sensing technology. Landslide detection and monitoring have been using some form of remote sensing to improve the accuracy since the inception of remote sensing in the civilian application(Cornforth 2005).

### *Data collection*

Before visiting the site, additional information must be obtained such as previous site investigations, construction activities on the property, topographic plans, aerial photos, historic landslide records or newspaper articles of past events of the location.

### *Site investigation*

This is the important part of the investigation and 75% of the final results depend on this step. The site investigation is generally done by 2 people one of them being the engineer or geologist. The reconnaissance can be completed in 2 hours for small landslide and approximately 8 hours for large landslides(Wieczorek and Snyder 2009). The site engineer first assesses the exact length of landslide and finds its boundaries. This is accomplished by using hand level, theodolite and survey rod. This data is generally correlated with aerial surveys. The next step involves boring a hole in the center of the landslide to assess the depth of slippage and determine other geological data like ground water level near the slip surface and collection of soil samples for lab tests. For wide landslides, additional boring lines are required. For some cases, additional field investigations may be required to provide additional subsurface data. These field investigations generally improve the accuracy of the previous test results. Site investigations are accurate and comprehensive but are time consuming and labor intensive. Although it is affordable when analyzing a single case this method becomes impractical for multiple cases.

# Chapter 2

# Brief Introduction to Remote Sensing

## Electromagnetic spectrum

Electromagnetic(EM) spectrum is the entire range of energies that are produced as a result of interaction between matter and energy. The different regions of the EM spectrum are distinguished with respect to the wavelength to: gamma rays, X-rays, ultraviolet rays, visible light, infrared rays, radar, FM, TV, shortwave and AM as illustrated in Figure 2.1.

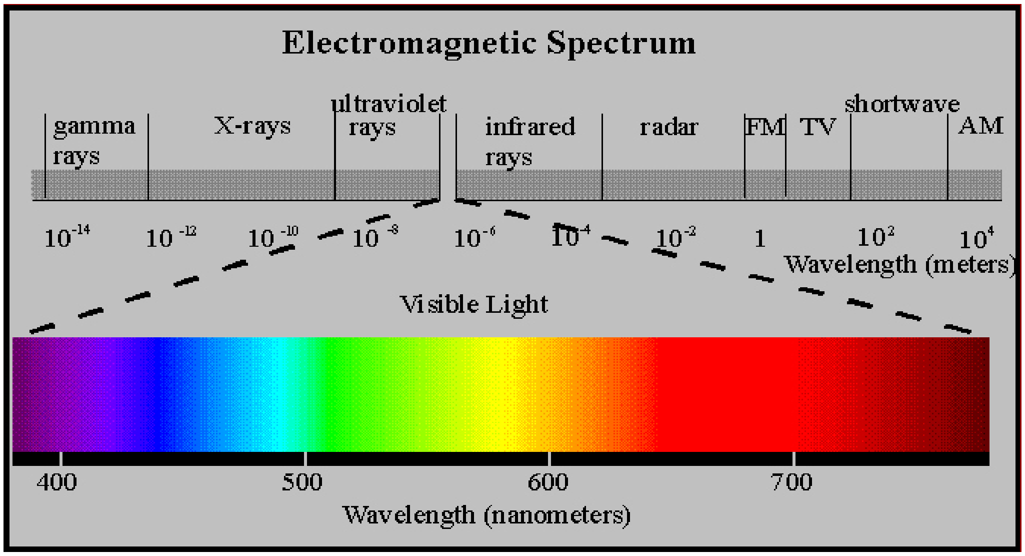

Figure 2.1: This picture represents the Electromagnetic (EM) Spectrum

This energy carried in EM waves when interacting with an object is the result of one or more of the following effects

Absorption (Eabsorption): This is the portion of the incident energy that is converted to internal energy in the object.

Scattering (Escattering): This is the portion of the incident wave that upon contact with the matter bounces off the object and propagates in multiple directions.

Emission (Eemission): This is the energy emitted by the matter, when its atoms fall from higher excited state.

Transmission (Etransmission) This is the energy that travels through the matter without effecting it in anyway.

When the incident wave energy is emitted by the sun, and in view of the aforementioned effects, the different regions of the EM spectrum interact with the earth as follows: The Gamma and X rays are entirely absorbed by earth's atmosphere. The part of the Ultraviolet rays (U.V.) in the wavelength range 0.03 – 0.4 micrometers is completely absorbed by the ozone layer. The remaining UV part in the wavelength range 0.3-0.4 μm is invisible to naked eye and behaves similar to visible light. Different parts of the visible light are reflected by matter and the color of the matter as seen by the naked eye is the reflected part of the light. The infrared rays are absorbed by matter as heat transfer. The radar waves in the wavelength range 0.1-100 cm are absorbed by the atmosphere, while the rest are transmitted through the atmosphere.

The interaction of EM spectrum can be better explained from fig 2.2 which shows how certain wavelengths of light interact with water ($H_2O$), Oxygen (O) and Ozone ($O_3$) as the figure describes different parts of spectrum have unique interaction behavior.

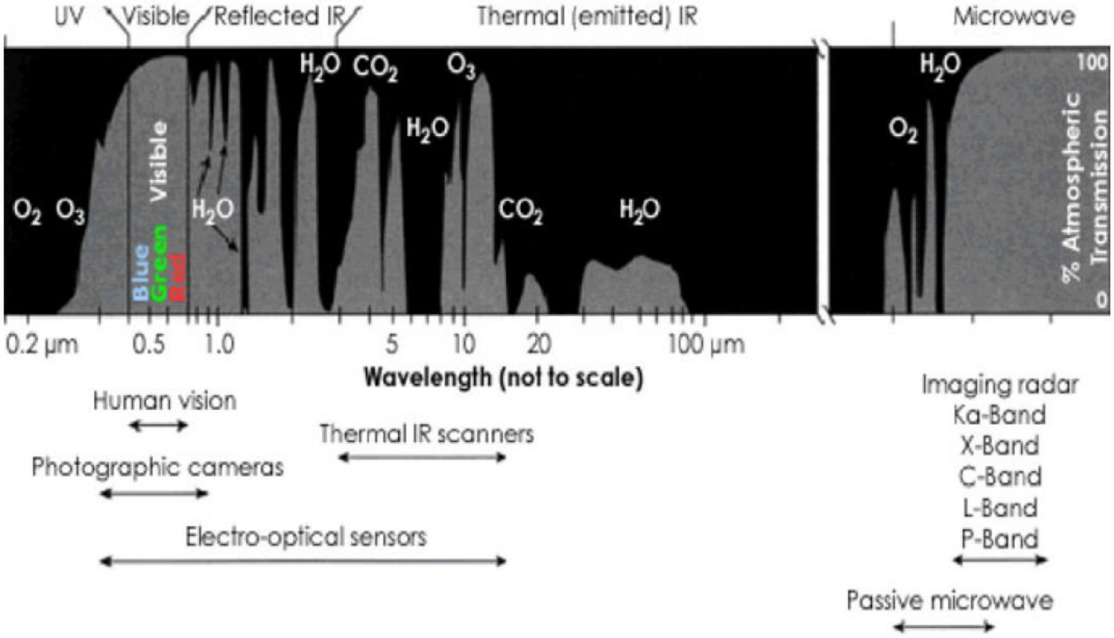

Figure 2.2: This image describes how different wavelengths of E.M. spectrum behave with water, oxygen and ozone. These omponents constitute most of the atmosphere (Pamela, 2009).

## Sensor

Sensor is a device that observes the interaction between 2 entities. In the field of optical sensors, they observe the interaction of E.M. waves with matter. These sensors can be divided into two types based on the origin of the energy source. If the source of the energy is not natural i.e. an instrument generates the energy, then it is called an active sensor. If the source of energy is natural, i.e. sun or the energy, $E_{emission}$, emitted by the target then this type of sensor is called a passive sensor. Most of the sensors observe the light interactions that are not visible to the naked human eye and the observations are developed in false color composites, so scientists can observe the necessary data.

The following sensors are used in landslide investigation. They are described based on type of sensor and EM spectrum interaction they observe.

### *HR/VHR*

High-Resolution (HR) and Very High-Resolution (VHR) images are acquired by passive sensors which observe visible light and have resolution of 30 meters and 60 centimeters, respectively. They are available onboard the *Landsat* and the *QuickBird* satellites (Munzer, 2010).

### *Panchromatic images*

Panchromatic images are in black and white but represent all the wavelength of visible light. These sensors are passive and have higher resolution compared to their counterparts in the visible spectrum (CRISP, 2017).

### *Multispectral*

Multispectral image contains the properties of the target beyond the visual spectrum, like I.R and U.V waves. These are observed by sensors which use additional filters and therefore are considered passive sensors. The resolution in these sensors differ from the visual spectrum as these images observe the absorption and transmission properties of the target (CRISP, 2017).

### *LIDAR*

LIDAR stands for Light Detection and Ranging. These sensors use laser (1550nm) to illuminate the target and measure the reflected pulse. Since the source of the light is by the platform these sensors are active sensors (GISGeography, 2017).

### *SAR*

Synthetic Aperture Radar (SAR sensors are similar to LIDAR but they use radar waves (0.1-100cm) and cover much larger area as compared to LIDAR. Since these sensors also include their own energy source they are active sensors (Ferretti et al. 2007b).

# Chapter 3

# Landslide investigation using remote sensing

Landslide investigation in the past few decades always used some form of remote sensing techniques. In this chapter, most of the remote sensing techniques and sensors are briefly explained.

Remote sensing in its most basic form can be described as observing or collecting data without having any contact with it. There are multiple types of sensors classified into 3 types based on their platform, i.e., ground-based, airborne and space-borne. It is important to integrate these techniques for landslide investigation as they would reduce the cost of manpower and it's easy to make early predictions with them and hence help in mitigating the damage caused by them(Scaioni et al. 2014). Landslide investigation is primarily divided into 2 groups, i.e., Landslide recognition and Landslide monitoring. Landslide recognition is the initial step and is generally followed by landslide monitoring and hazard analysis.

## Landslide Recognition

Landslide recognition involves all activities required to detect landslides in a specific region. These involve analyzing past events, building inventories etc. This step does not involve detection of a single landslide, but rather the mapping of the location of multiple landslides in each area. Most of the techniques that are described depend on the principle that landslide events cause a disturbance in the area. These changes can be detected by aerial or satellite images as there will be a change in the topography which can then be taken as a mark of slope instability. These techniques are considered novice or basic and are useful to find shallow landslides or instabilities, whereas much more complex methods are used for deep-seated landslides. Some of the sensors and techniques used in landslide recognition are also used in monitoring, however the acquisition frequency and application differ.

Landslide recognition is discussed next based on the technique used for detection rather than the sensor, as different sensors are used within the same technique

### *Visual interpretation and geomorphic feature extraction*

This is the most commonly used technique in landslide recognition due to the high-quality images that are obtained from High Resolution (HR) and Very High Resolution(VHR) sensors that can cover large areas. This interpretation technique is based on the concept that certain characteristic changes in a target location can be attributed to landslide activity. The sensors used in this technique mostly depend on the visible region of spectrum and photogrammetry. This technique revolves around the fact that most landslides cause a topographical change which can be detected over a period of time.

A sensor takes multiple pictures of a location. These pictures are approximately of size 21cm X 21cm and scale from 1:5000 to 1:70000 from these images a trained geomorphologist can detect a change in the images. This technique is effective when considering the satellite orbit as the images can be taken at required intervals and the change detection is more optimized (Guzzetti et al. 2012). Fig 3.1 shows the application this technique to detect landslides.

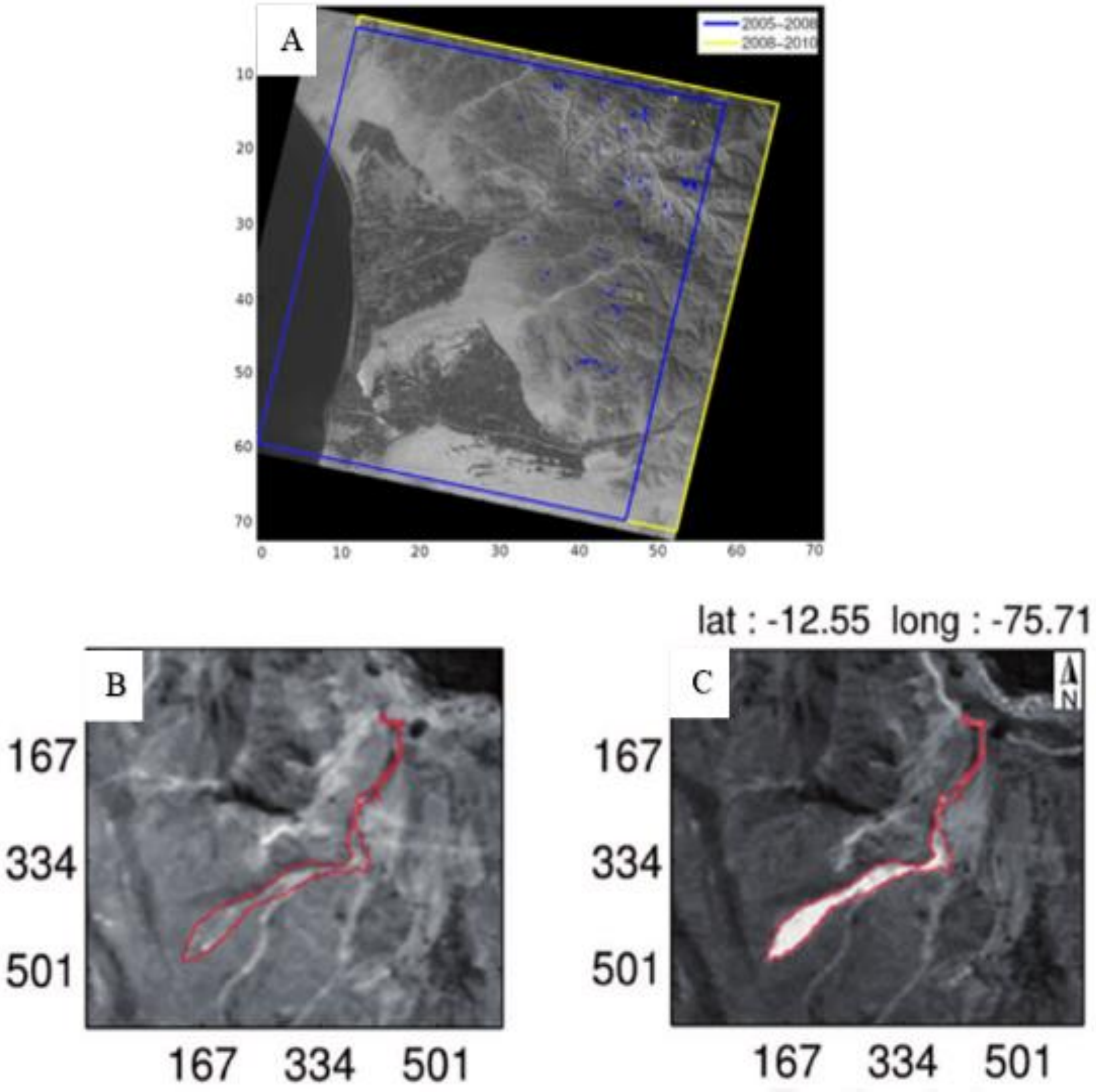

Figure 3.1: In image A, combination of visual interpretation and automatic pixel recognition methods are used to detect landslides. Images B and C show the landslide detected using the above method. Image B shows the location before the event and image C shows the landslide after the event(Lacroix et al. 2013).

Example

In this study(Fiorucci et al. 2011) the investigators had problems getting timely post event aerial photographs. They tackled this problem by using HR and VHR optical images. The study area in this experiment is 90km$^2$ in central Italy, Umbria which has been experiencing high landslide activity. The study was performed using IKONOS satellite images along with Terra Italy aerial photographs. The investigators found a total of 161 landslides from IKONOS out of which 13 new landslides were not detected by Terra Italy. Some of the landslides detected are shown in fig (3.2). The study concluded by proving that visual interpretation of aerial and satellite image is more accurate than preexisting reconnaissance inventory obtained through unsymmetrical field surveys.

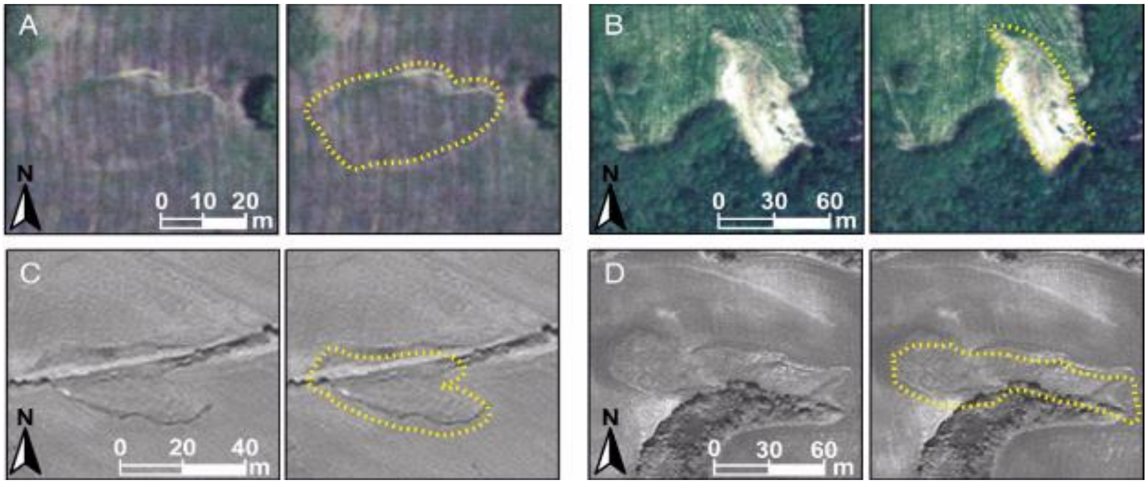

Figure 3.2: Images of landslides recognized by color ortho-photographs (A and B) and panchromatic images (C and D). The yellow lines highlight the detected landslide. (Fiorucci et al. 2011).

*Image fusion technique*

The images obtained from the satellite are improved by using the technique called image fusion. This is a technique in which 2 images are merged to obtain a better image. This is extremely useful in landslide investigation as the image obtained from a satellite the first time may not be accurate to be able to detect the change in topography. Image fusion techniques are not only used to improve the quality of the image but this technique is primarily used to combine two images which have distinct spatial and spectral characteristics. The resulting hybrid image will have characteristics of both parent images. This technique is implemented because the image resolution changes for different spectral ranges, even though they are taken from the same satellite(Lu et al. 2011). Using image fusion, a high-quality panchromatic image can have additional spectral information imbued into it which can make the observation of landslides from these images easier. In Fig (3.3) HIS Image fusion technique (Marcelino, Formaggio, and Maeda 2009)is used to detect landslide.

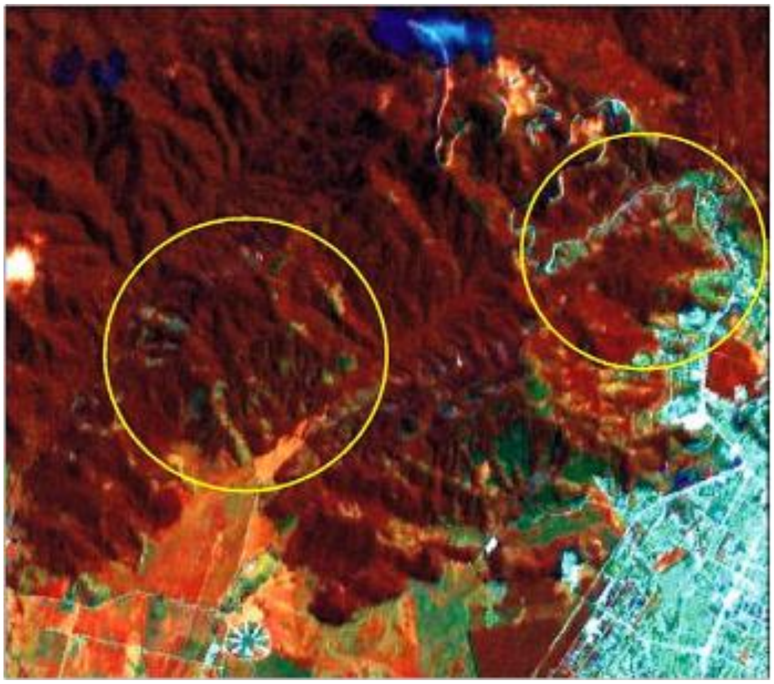

Figure 3.3 : In this image landslide were detected using IHS image fusion technique. (Marcelino, Formaggio, and Maeda 2009)

Example

In this study (Wong, 2005) a 36km$^2$ heavy landslide area on Lantau island, Hong Kong was investigated. The investigators used automatic change detection technique to detect small landslide from medium resolution SPOT images and used image fusion technique for qualitative interpretation of landslides. Multispectral images of lower spatial resolution were fused with panchromatic images of higher spatial resolution. To achieve this effectively four-image fusion techniques were used namely, the IHS method (Mathew, 1999), the Brovey transform method (Gillespie, 1987), the smoothing filter modulation method (Liu, 2000) and pan sharpening (Zhang, 2002). From the methods tested the pan sharpening method was found to be most effective because the fused image from pan sharpening was the least spectrally degraded and it contained the maximum information. Fig (3.4) shows the landslide detection using image fusion technique from pan sharpening.

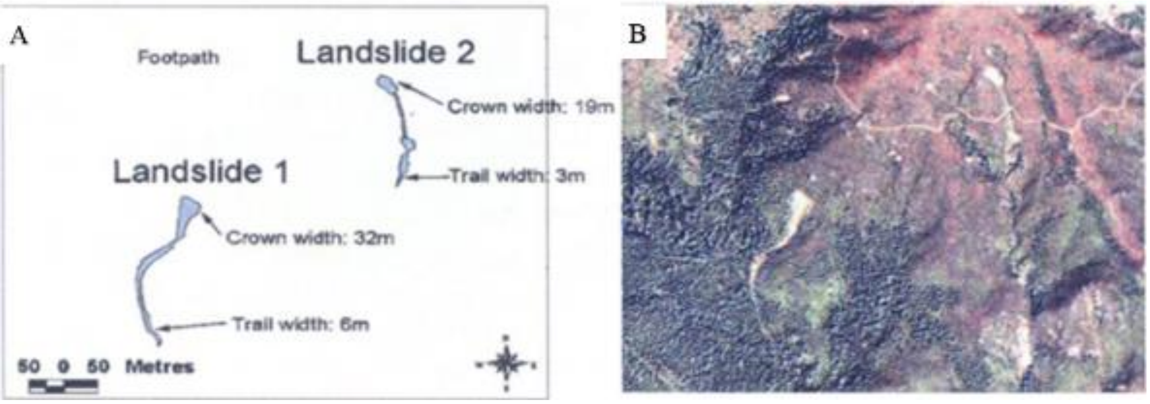

Figure 3.4: The above image (A) shows the detected landslides and the corresponding pan-sharpened fusion image (B) (Wong, 2005).

*Stereovision*

Stereovision is a process of creating a three-dimensional (3D) image from two images taken at a certain distance from each other. This technique uses the same concept used by our eyes to create a 3D view. For landslide recognition two images are calibrated and are processed using a stereometric program to create 3D image. This process is sometimes done using a special device from which a geomorphologist is capable of detecting landslide. The landslide generally looks like sliding of ground or flow pattern and can be seen in fig (3.5) shown below(Alkevli and Ercanoglu 2011). It should be noted that detecting landslides using this method depends on the experience and training of the geomorphologist and is unreliable as there does not exist any actual standards. But this technique does not require any sophisticated technological skills and is widely used. This is also due to the fact that recent advancements in computers have improved assisted stereovision(Haeberlin 2003).

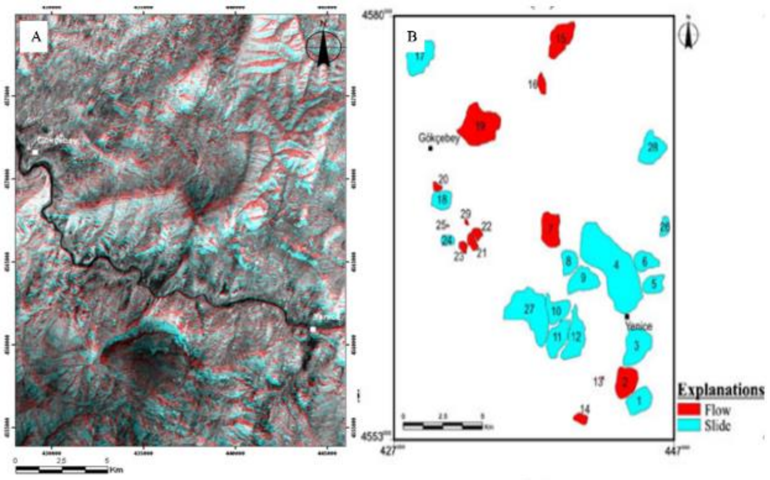

Figure 3.5: The image (A) represents the stereo image used to detect landslides. The landslides detected using image A are shown image B (Alkevli and Ercanoglu 2011).

Example

This study area(Murillo-García et al. 2015) is in Puebla central Mexico and covers 54Km$^2$.The region is a mountainous terrain. The investigators performed visual analysis of stereoscopic pair VHR satellite images. Geo Eye-1 stereoscopic pair images with spatial resolution on panchromatic band were used. To improve the 3D models a computer software was used to assist in identification of landslides. The investigators were able to detect 390 landslides using stereoscopy and additional landslides were later detected by field survey. Stereo mirror system and landslide detected is shown in fig (3.6).

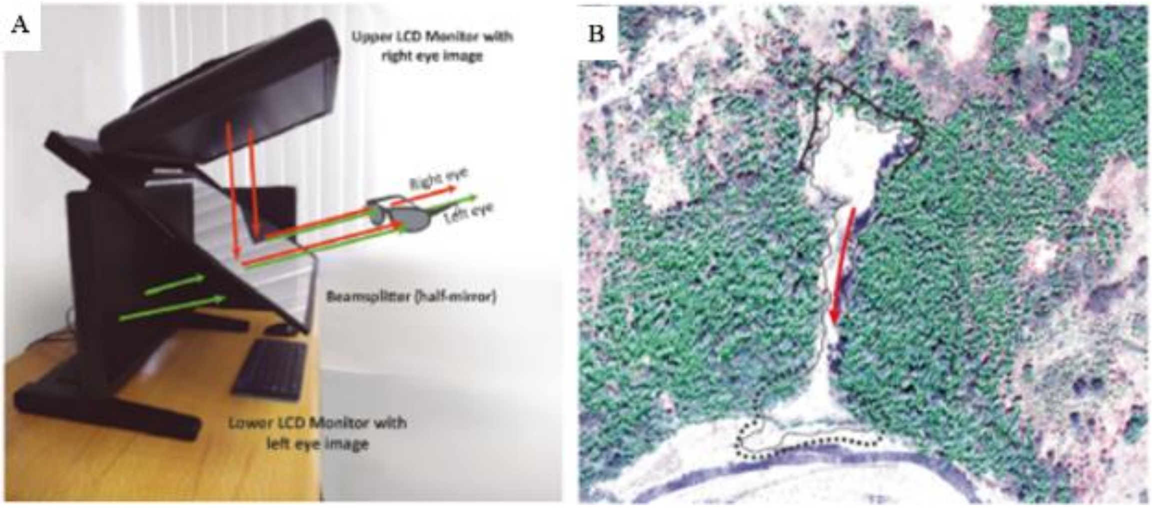

Figure 3.6: Image A shows the stereo mirror system to view stereo image. Image B shows the landslide DEM from GeoEye-1 stereo pair (Murillo-García et al. 2015).

### *LIDAR*

LIDAR stands for LIght Detection And Ranging, it is a remote sensing technology that uses light reflection to obtain the x,y,z coordinates of the target location. LIDAR exist in both terrestrial and airborne format but for landslide recognition, they are used on board an airplane or satellite. When the sensor flies above an area it fires a laser at the location. As the light is reflected back the distance between the sensor and the location is found and this technique a highly accurate image is obtained. The image is then processed and a Digital Elevation Model (DEM)(appendix) is created for visualization and spatial analysis. From the DEM, a landslide can be detected by a geomorphologist or by assisting program. The landslide described in fig (3.7) is obtained using similar method. The additional benefit of using a LIDAR DEM is that the complete displacement field for the whole landslide is obtained as compared to point measurement (Jaboyedoff et al. 2012). This process is better explained in the following example.

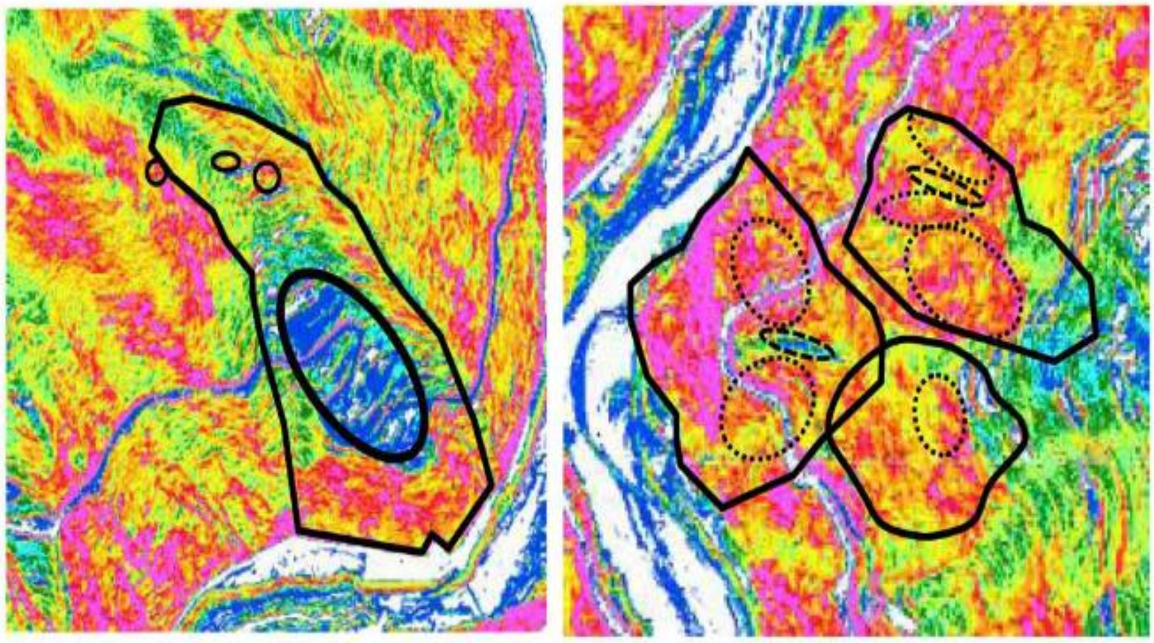

Figure 3.7: Deep seated landslides are detected from eigenvalue and slope filter ratio obtained from airborne LIDAR. The image above represents the spatial distribution of slope angle (Kasai et al. 2009).

Example

The region(Chen et al. 2014)is located near Shazhenxi town China and covers an area of 21.6Km$^2$. In this study, the LIDAR derived topographic images (fig 3.8) were used along with field investigation and visual interpretation of aerial images. The study concluded that some new features can be extracted from LIDAR derived Digital Terrain Model (DTM) and proved that LIDAR is not affected by topographic shadowing which generally effects radar type images.

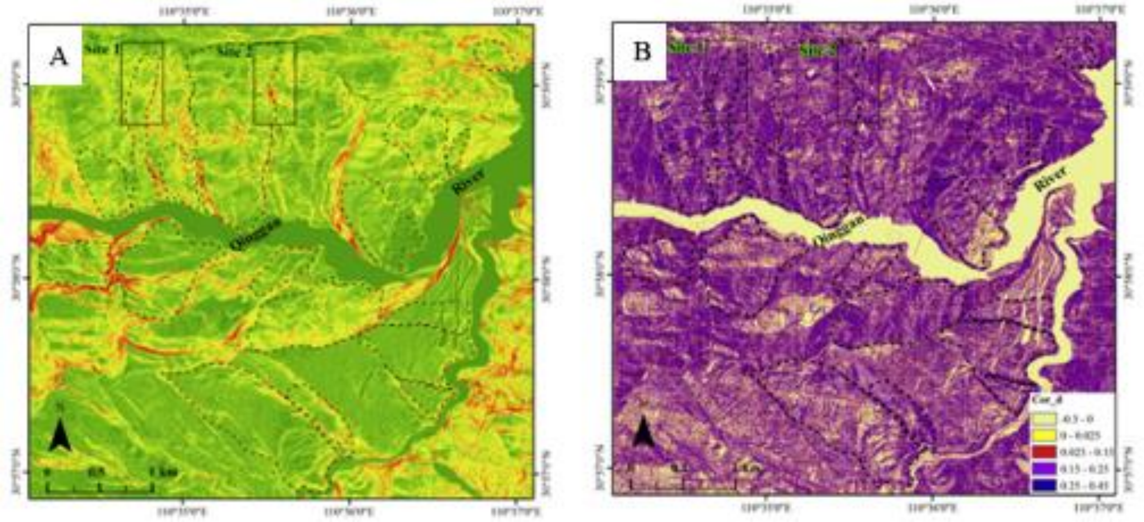

Figure 3.8: Image A shows the moving average filter map for slope and landslide. Image B shows the average correlation texture map for DTM and landslide locations. landslides in both images are marked by dotted line (Chen et al. 2014).

*Automatic landslide recognition*

Automatic landslide recognition is a not a new concept in landslide recognition but due to the possibilities of error, human oversight has been necessary. The technique is pixel based i.e. the computer program involved analyses of each pixel from RS data and detects changes that are related to landslides. This method in most studies has been known to introduce numerous errors as seen in fig (3.9) (Moine, Puissant, and Malet 2009). New studies conducted in the past decade have taken a new approach in which the algorithm involved switched to object-based study instead of pixel based study. This improved the accuracy as the algorithm treats the landslide as aggregation of pixels instead of spatially unrelated cells (Blaschke 2010). This can be observed in the following example.

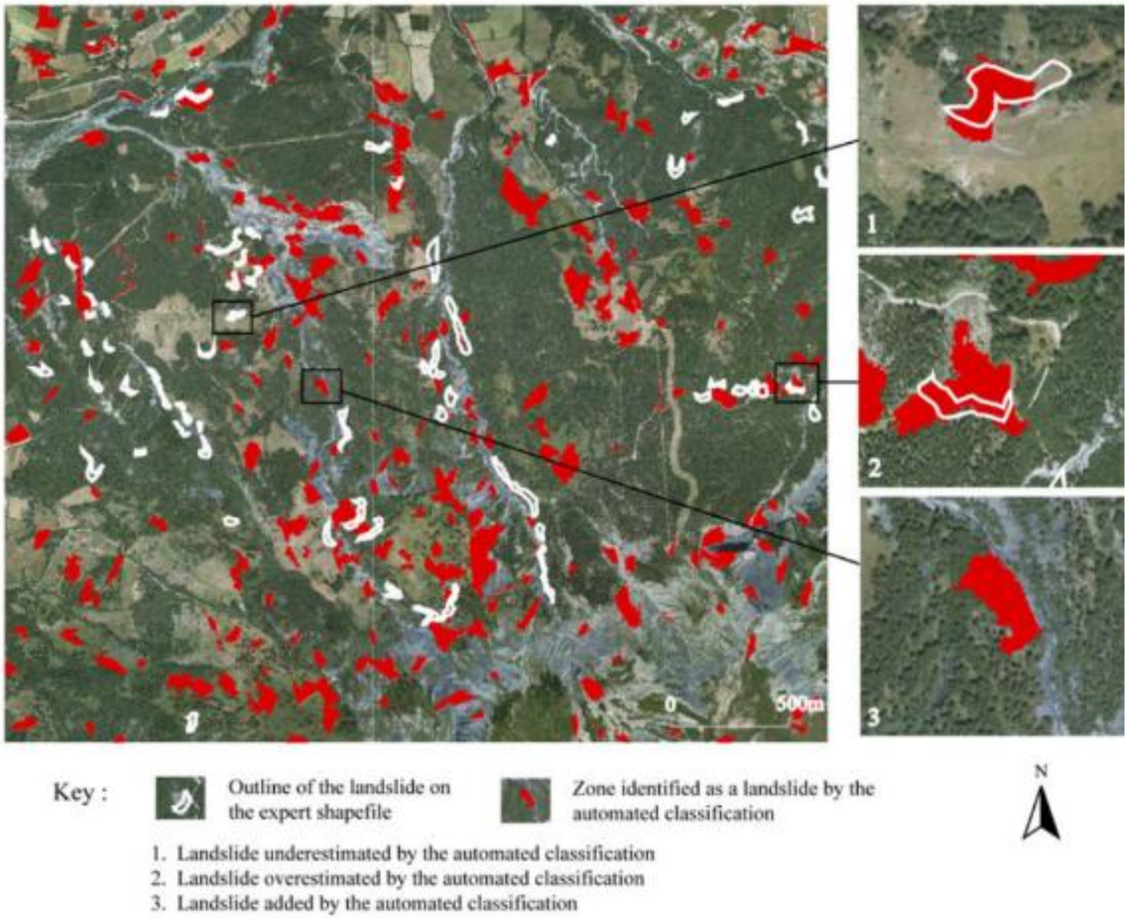

Figure 3.9: As the key indicates the above image represents the landslides detected from semi-automatic landslide methods along with some false positives (Moine, Puissant, and Malet 2009).

Example

This study(Lu et al. 2011) was conducted in Messina province of Sicily, southern Italy. The area was affected by intensive prolonged rainfall which triggered numerous landslides (shallow and debris flow). Two areas which were most damaged were surveyed for this study. Two Quickbird images with zero cloud cover were used. The landslides detected using automatic approach were compared with manual landslide inventory. Their accuracy was compared on number and spatial extent of mapped landslides. From the method used the automatic algorithm detected 242 landslides and manually 285 landslides were detected. This technique was proven to be effective with few false positives as exceptions as can been in the fig (3.10) where both the landslide and the false positives are highlighted.

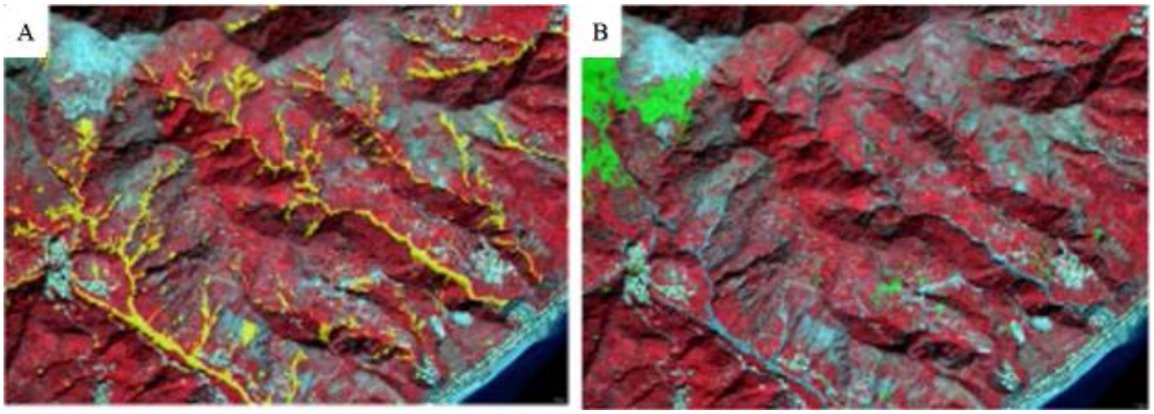

Figure 3.10: image A shows the final result of the landslides detected using the automatic method marked in yellow. image B shows the false positive obtained from this method marked in green (Lu et al. 2011)**.**

*InSAR*

InSAR is Interferometric Synthetic Aperture Radar a technique which uses SAR sensors to recognize landslides. An SAR sensor is an active microwave sensor which records the radar echo from the target location. The SAR sensor uses one of the three bands available, i.e., C, L, and X which have a wavelength of 5.6cm, 23.6cm and 3.1cm, respectively(Thomas M. Lillesand, Ralph W. Kiefer 1989). InSAR technique detects landslides by calculating an interference pattern which is obtained from the phase difference between two SAR images at required intervals. The phase difference contains possible ground displacement along with other “Noise” which can be reduced / eliminated if the coherence between the two images is high.

Differential Interferometric Synthetic Aperture Radar (DInSAR) is an InSAR technique which removes topographic noise from two SAR images to extract the displacement pattern This is visible in fig 3.11(Guzzetti et al. 2009).

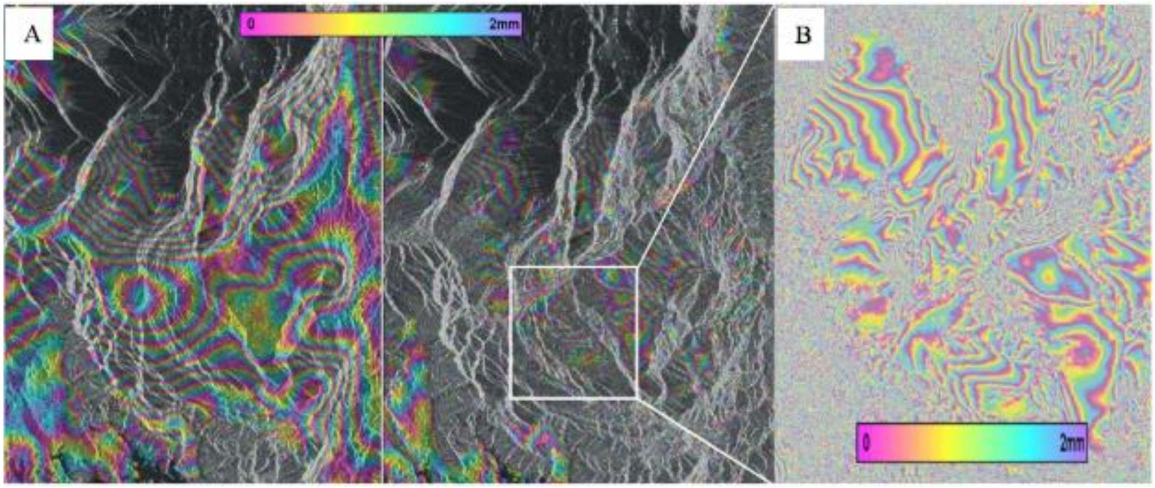

Figure 3.11: The above images represents the fringe pattern from InSAR .2 pass processing in A, 3 pass processing in B and enlarged image representing movement rates around 14mm in 3 months (A.Walther, 2008)**.**

Example

This study (Christophe Delacourt et al. 2009) was performed in La Reunion island which is in Indian ocean which experiences constant slope movement and huge landslide activity due to climate and topography. DInSAR analysis was carried out using Radarsat C-band images and Jers-1 L band SAR images. From the research, it has been shown that the L band SAR images have a prominent application in the future. It has also been stated that lack of archive significantly reduces the effectiveness of such studies as more acquisitions improve the results. Results from C-band and L-band are shown in fig (3.12)

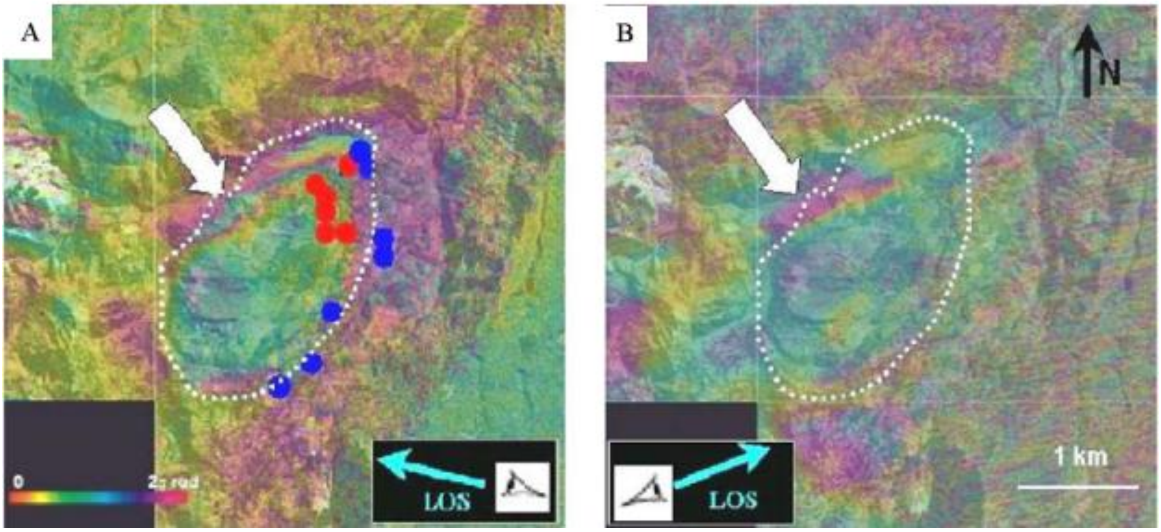

Figure 3.12: The above images represent the landslides detected from (A) C-band satellite and (B) L-band satellite. The arrow indicates the unstable area which is visible in both the images (Delacourt et al. 2009).

### *Thermal InfraRed*

Out of all the techniques mentioned here, TIR is the least promising technique and can only be used in very rare cases. This is due to the constant change of temperature of the target location nearly every day due to weather, soil, climate etc. Theoretically, the concept behind this method is that some landslide activity is directly related to soil moisture and saturation which is directly proportional to the temperature of the soil. The sensor calculates this, and landslide risk can be estimated. This technique has been successively used to map glacier-related landslides like rock and ice avalanches as changes in these types of landslides can be easily be detected from thermal sensors (Weng 2009).

## Landslide monitoring

Landslide recognition is just the first part of the investigation. These landslides must be observed over a period to observe their condition and to see if there is a potential to change. This change can be in their size or condition. This form of observation is called landslide monitoring. Landslide monitoring is handled through qualitative assessment of the general conditions of a landslide-prone slope along time, or through the quantitative measurement of ground deformation and surface point displacements. Since most of the remote sensing sensors revisit at regular intervals observing these progressive deformations is ideal. The techniques in landslide monitoring are comparison based studies and some of these techniques are automatic or semi-automatic and discussed next.

### *Digital Image Correlation*

This is an advanced technique that uses a combination of other techniques to preprocess the images after which this technique is applied to monitor the target location.

#### Preprocessing

Two stereoscopic images of the location are first obtained each with a time gap as large as of several years depending on the monitoring frequency. Both images must be taken from the same height. For successful correlation, the images must be of same geometry and orthorectification to both images must be done, after which, the two DEMs are developed and Digital Image Correlation can now be conducted.

#### Methodology

To quantify the ground displacement a correlation window is defined to the oldest image, the size of which depends on the accuracy of the displacement required and the spatial resolution of the velocity field (velocity of an element of fluid at a time). This window is searched on the newest image to increase the correlation function. The ground displacement is the measure of shift between the 2 acquisitions by the pixel size(Travelletti et al. 2012). This process is repeated for each pixel until the complete displacement field is obtained. This concept can be better understood from the example below.

Example

In this study (C. Delacourt et al. 2004) two aerial stereoscopic image pairs have been acquired over four years apart. The study area is 36 Km$^2$ and is located in French Southern Alps. The landslide investigated is called “La Capiere”. The investigators applied optical correlation technique to derive deformation maps of landslides that have continuous deformations. This is seen in fig (3.13). The study also concluded that the limitation of DInSAR can be overcome if used in combination with optical correlation.

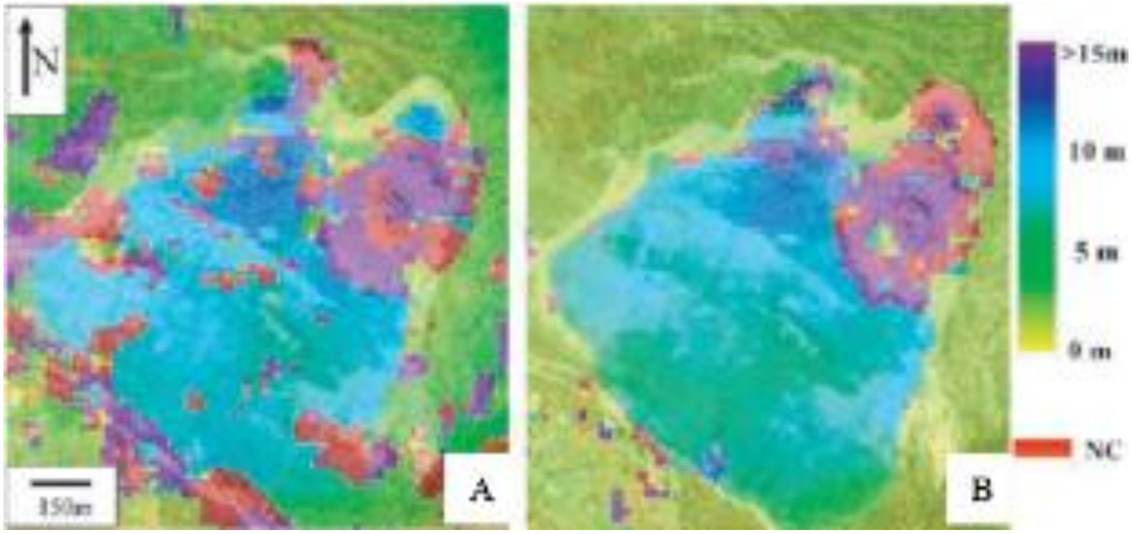

Figure 3.13: Displacement map obtained by correlation between aerial photographs. A is the displacement map between 1999 and 2003 and B is the displacement map between 1995 and 1999. NC from the scale represents no significant displacement because of poor correlation values(C. Delacourt et al. 2004).

### *Comparison of HR-DEM*

For this technique, high-resolution images are taken from which DEM are created. The high-resolution images can be taken from satellite images or laser scanning techniques are also used(Brückl, Brunner, and Kraus 2006). In the case of a terrestrial laser, a station is built opposite the location to range accurately. Since the station can measure the reflection of light regularly, the landslides displacement is computed by comparing the DEM at regular intervals(Bitelli, Dubbini, and Zanutta 2004). This technique is explained by considering following terrestrial laser scanning example.

#### Example

In this study(Corsini, A and Cervi, F and Daehne, A and Ronchetti 2009) Trafoi landslide in South Tyrol (Italy) is investigated. To obtain High resolution DEM the investigators used LIDAR devices equipped on a Helicopter, the test area was surveyed three times between 2005-2007 fig (3.14). The HR DEMs have been used to estimate surface roughness that helps in understanding the landslide internal activity. The researchers have concluded from this study that the comparison of multitemporal DEM were useful for calculating depletion and accumulation at the slope scale. Fig (17) shows landslide development and the outline of the landslide area when the area was investigated.

### *SAR interferometry*

#### Spaceborne

In the last two decades, advanced Differential Interferometric SAR techniques have been successfully used to monitor slow-moving landslides. This is due to the fact that large stacks of data are available as the satellites take images continuously at regular intervals as they follow their orbit. This process also improves the coherence between the images. The time period between each image depends on the user as the latest satellites have an orbit period of 2 days (Cosmo-sky med). The displacement that can be detected by this method is equal to 0.25 wavelength of SAR sensor. therefore, a sensor with X-band can observe a displacement of 8mm(Cascini et al. 2010).

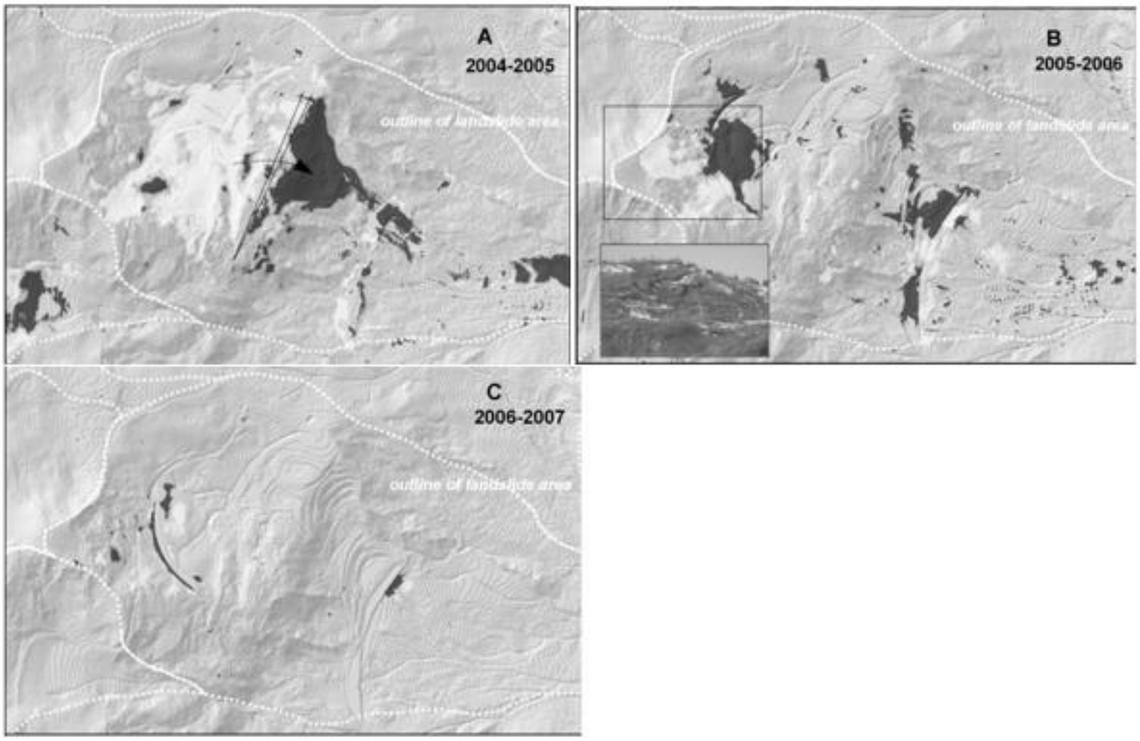

Figure 3.14 DEMs obtained from LiDAR datasets show the landslide. The dotted line points the outline and progression of landslide in years A (2005), B (2006), C (2007)(Corsini, A and Cervi, F and Daehne, A and Ronchetti 2009) **.**

Example

This study (Bianchini et al. 2013)was conducted in Tramuntana Range, Majorca(Spain). The investigators used PSInSAR to generate Landslide activity map fig

(3.15 (A)). The acquisitions needed were taken from L band, ALOS sensor and a total of 14 number of acquisitions were performed. From the analysis, the investigators concluded that using L band SAR data detection of ground movement is faster as compared to C band. Finally, the investigators were successfully able to monitor each landslide and assign its respective velocity. Fig(3.15) show the landslide inventory maps being developed using PSInSAR and statistical evaluation of database.

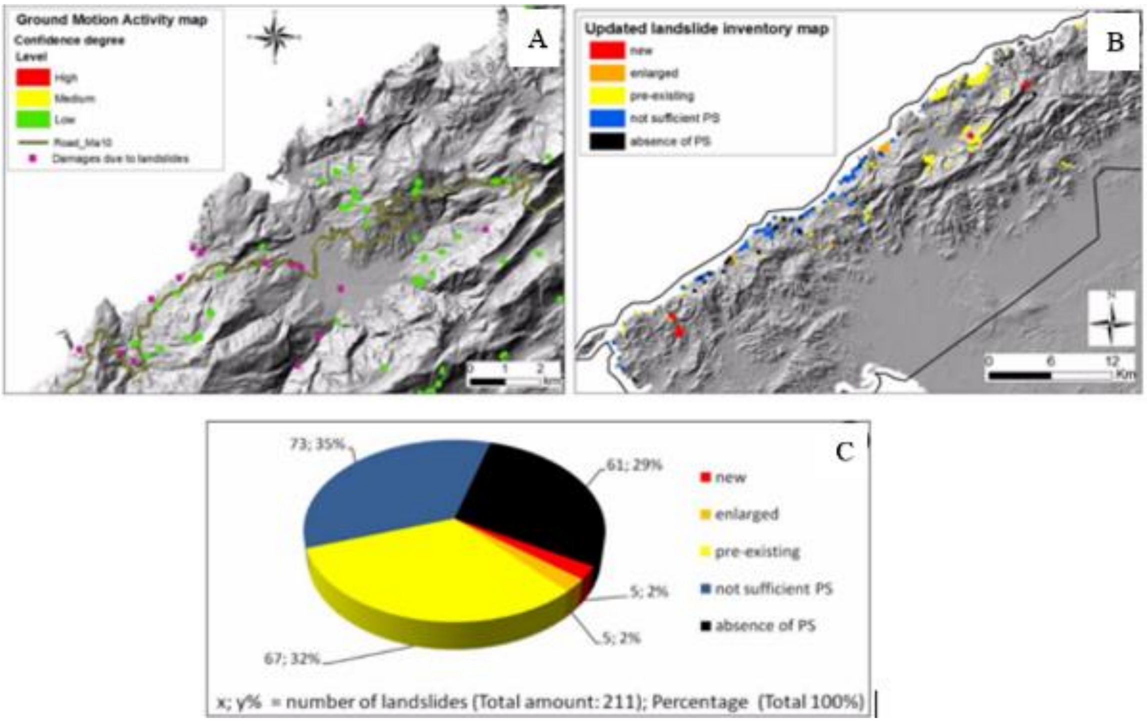

Figure 3.15: (A) represents the ground motion activity detected by PSI. (B)Landslide inventory map updated in Tramuntana Range with (C) representing the statistical evaluation of landslide database improvement (Bianchini et al. 2013).

## Terrestrial SAR Interferometry

Terrestrial Interferometric Synthetic Aperture Radar (TInSAR) is a ground based radar technique that is used to monitoring the displacements. TInSAR is performed by placing radar sensors on rail and taking acquisitions of target area from two different sensor locations. From the two acquisitions, interferometric techniques are applied to develop DEM and obtain displacement maps(Tarchi et al. 2003). The accuracy in this method is greater than space based interferometry as the signal to noise ratio is very high in this method due to short baseline and short monitoring distance. This technique is not restricted to landslide investigation but also in the displacement analysis of man-made structures like buildings and roads (Paolo M, 2015).

Example

In this study(Tarchi et al. 2003) the landslide Tessina located in North Eastern Italian Alps was monitored using ground based SAR system. The SAR installation (fig 3.16 (A)) was used for early warning purpose as the landslide showed signs of being active again and it posed risk to nearby villages.

The landslide was monitored using a portable SAR instrument. From the data that is obtained, DInSAR technique (fig 3.16(C)) was used to monitor the landslide with millimeter accuracy. The data obtained is used to monitor the kinematic and short-term evolution of the landslide. The investigators concluded that ground based. SAR has numerous advantages to its space based counterpart and further application is needed taking these advantages in mind. In the fig (3.16) the experimental set up of the TInSAR is shown along with the DEM generated by the machine.

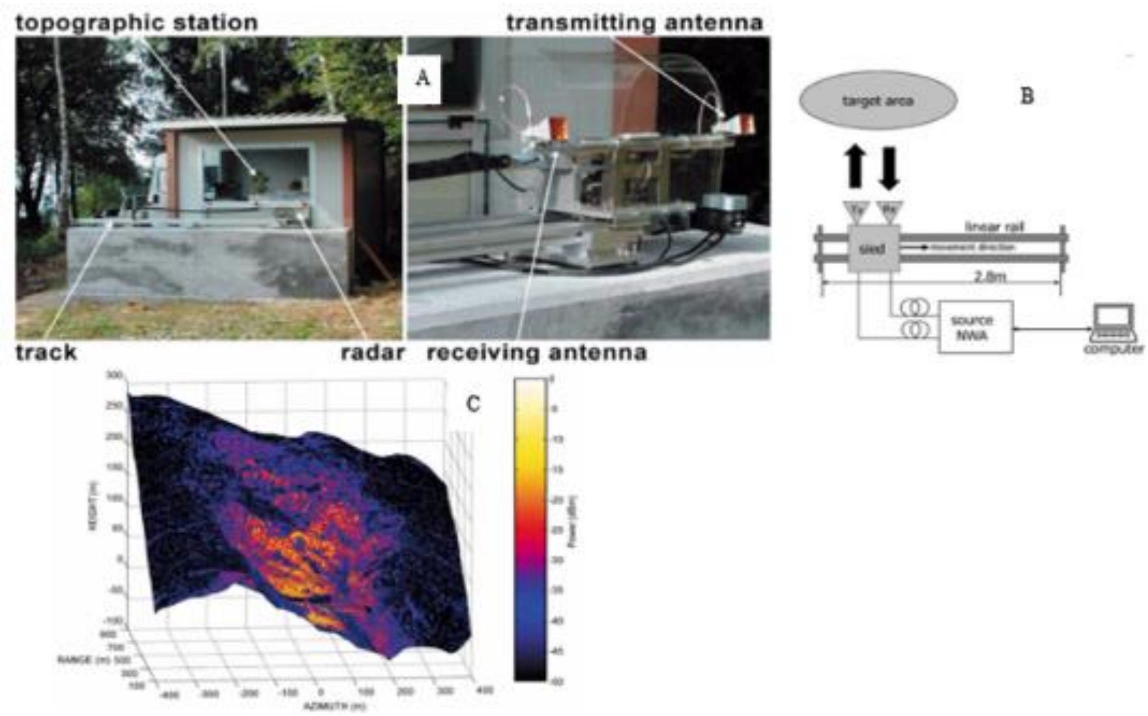

Figure 3.16: (A)represents the field set up of instrumentation (B) shows the technical scheme the equipment (C)shows the DEM of the target scene projected represented in local coordinate system with center being the point of origin (Tarchi et al. 2003)

### *Techniques used for different types of landslides.*

All of the R.S techniques mentioned above cannot be used for each of the mentioned landslides because each has its own unique failure mechanism. Table 3 provides the technique used for some of the common types of landslides described by Varnes. Most of the remote sensing techniques are mentioned in this review are described along with their potential to be automated. Some of the techniques mentioned need to be integrated with multiple sensors these techniques are also mentioned in the table.

Table 3.1 : Landslides and Remote Sensing techniques to investigate them

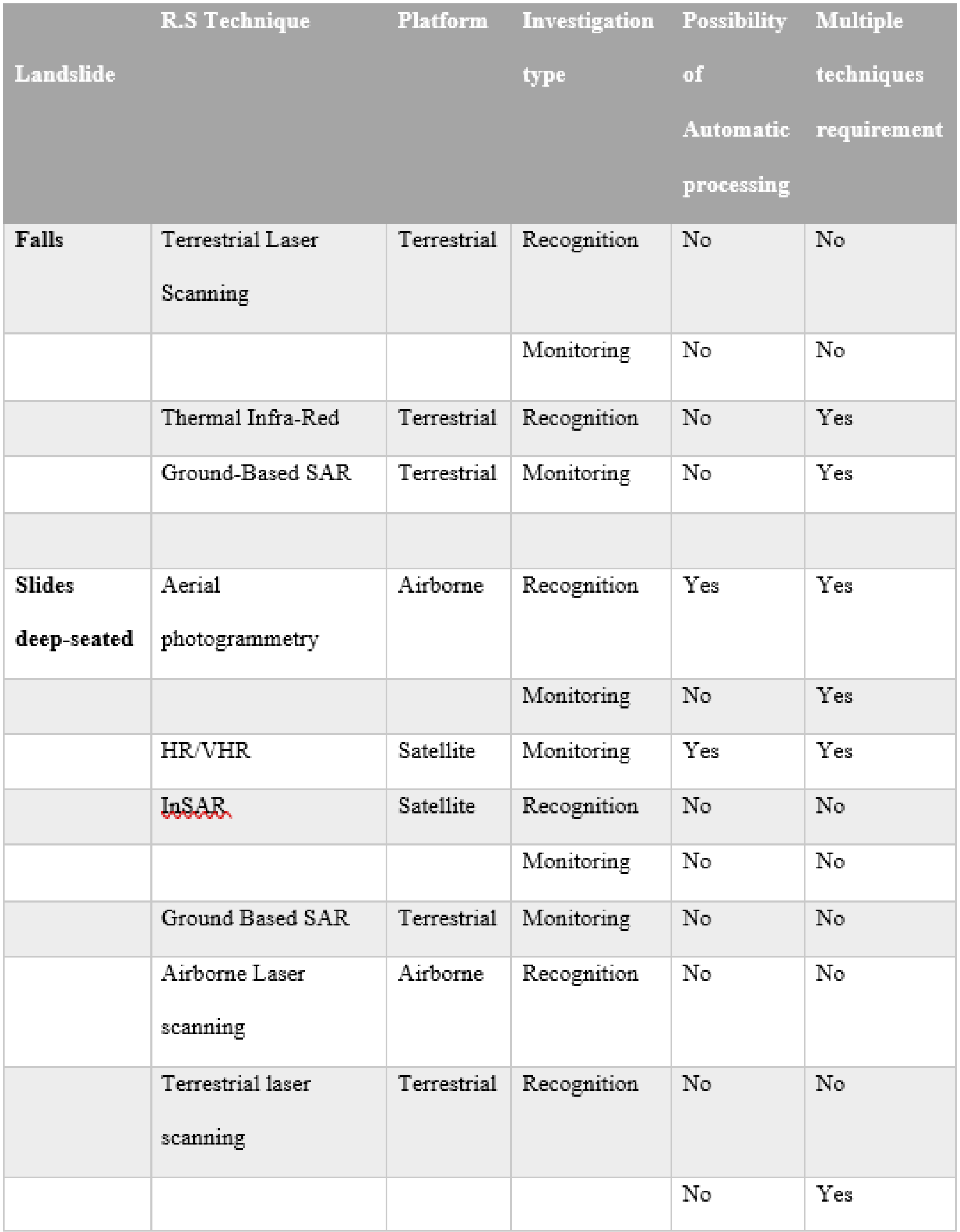

| Landslide | R.S Technique | Platform | Investigation type | Possibility of Automatic processing | Multiple techniques requirement |
|---|---|---|---|---|---|
| **Falls** | Terrestrial Laser Scanning | Terrestrial | Recognition | No | No |
| | | | Monitoring | No | No |
| | Thermal Infra-Red | Terrestrial | Recognition | No | Yes |
| | Ground-Based SAR | Terrestrial | Monitoring | No | Yes |
| | | | | | |
| **Slides deep-seated** | Aerial photogrammetry | Airborne | Recognition | Yes | Yes |
| | | | Monitoring | No | Yes |
| | HR/VHR | Satellite | Monitoring | Yes | Yes |
| | InSAR | Satellite | Recognition | No | No |
| | | | Monitoring | No | No |
| | Ground Based SAR | Terrestrial | Monitoring | No | No |
| | Airborne Laser scanning | Airborne | Recognition | No | No |
| | Terrestrial laser scanning | Terrestrial | Recognition | No | No |
| | | | | No | Yes |

| | | | | | |
|---|---|---|---|---|---|
| | | | Monitoring | No | No |
| | | | | | |
| **Slides Shallow** | Aerial photogrammetry | Airborne | Recognition | Yes | No |
| | HR/VHR | Satellite | Recognition | Yes | Yes |
| | Airborne Laser scanning | Airborne | Recognition | No | No |
| | Terrestrial laser scanning | Terrestrial | Recognition | No | Yes |
| | InSAR | Satellite | Recognition | No | No |
| | | | | | |
| **Flows** | Aerial photogrammetry | Airborne | Monitoring | No | Yes |
| | InSAR | Satellite | Recognition | No | No |
| | Airborne Laser scanning | Airborne | Recognition | No | Yes |
| | | | Monitoring | No | Yes |
| | Terrestrial laser scanning | Terrestrial | Recognition | No | No |
| | | | Monitoring | No | No |

# Chapter 4

# Using InSAR for Landslide Recognition

## Introduction to InSAR

First satellite with Synthetic Aperture Radar (SAR) capabilities was launched on 27 June 1978(SEASAT) the same year as Navstar first GPS satellite. Experiments conducted by US jet propulsion laboratory showed that Interferometric InSAR was effective in monitoring changes but conducting additional research was difficult as more data was not readily available, and the computer technology was not advanced enough for easy processing of data. Around the same time the GPS technology gained traction and more advancements were made in its direction due to funding from US Department of Defense (USDoD). In the 1990's pioneers like Massonnet (Massonnet, 1990) showed multiple applications of SAR which brought new interest to the field, but the development was still slow as compared to other satellite technologies like GPS. This was due to application of InSAR required strong understanding of computer radar technology and geophysics, which was not usually the case as both topics were considered to be unrelated to each other. It is only in the last 2 decades that collaborations between radar specialists with geologists, civil engineers and other related disciplines has brought this technology to the spotlight. In 2014 SENTINEL-1A was launched which is the first civilian sensor specifically designed for monitoring deformations over large areas. This can be considered the crown jewel in the development of InSAR(Ferretti et al. 2007a).

## InSAR methodology

To understand how InSAR works it is imperative to first understand the basics of imaging with radar sensors and SAR

### RADAR Sensor

The major difference between an optical imaging sensor and a Radar imaging sensor is the wavelength at which they operate. The optical sensor operates at wavelength of approximately 1($\mu$m) and the Radar sensor in the range 4 cm- 10cm. A reference scale of the E.M spectrum is shown in fig 4.1 where it is evident that there exists significant difference in wavelength. The difference in wavelength implies that each sensor acquires images in a different way. For the optical sensor, the light waves cannot penetrate the surface and the image obtained would be either clouds or the surface landscape. But in the case of Radar sensor the longer wavelength implies that the waves can penetrate some media, including water, very dry soil, trees and clouds, among others.  The ability to penetrate increases with increase in wavelength. This property makes the radar imaging the preferred technique for some applications that cannot be done by optical imaging sensors (Richards, 2009). The energy source needed to view the target area is different for a Radar sensor. While the optical imaging uses the sun’s visible and infrared light, the radar sensor transmits its own “light” to “illuminate” the target area as seen in the fig (4.2) (Richards, 2009). where the energy emitted from the antenna illuminates the earth gets back to the platform. This is because the microwave energy transmitted by the sun and earth is too weak to be detected by the radar sensor to obtain meaningful data.

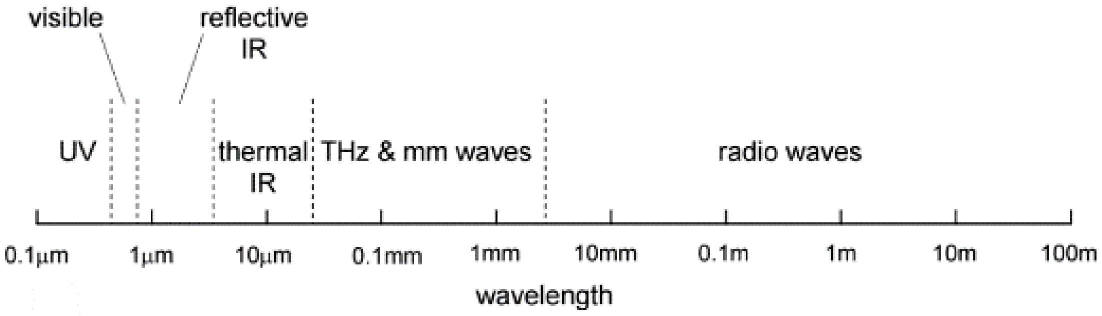

Figure 4.1: This is the reference scale for the E.M spectrum based on wavelength of light.

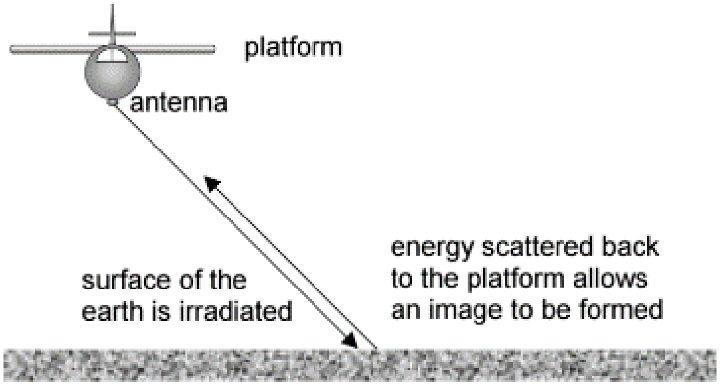

Figure 4.2: This image shows the working of an active radar sensor which illuminates its target with its own energy.

*Radar system*

The active Radar system used for remote sensing consists of a transmitter and a receiver (Ferretti, 2014) and are classified as *monostatic*, i.e., both the transmitter and receiver share same antenna, and *bistatic*, i.e. transmitter and receiver are located separately on the platform.  The monostatic remote sensors are widely used for remote sensing applications as compared to bistatic. The best approach to acquire an image with optical systems is to scan an area across the earth that is normal to system. However, this approach is not suitable for Radar systems as using this scan approach would result in lower resolution and smaller wavelength, as the beam would be narrow. Instead the radar system scans to its side as observed in fig 4.3 which shows longer footprint as compared to scanning normal to the platform (Richards, 2009). The pulse emitted by the radar, travels to the target at approximately speed of light, scatters and returns back to the system at the same speed. The returned pulses are separated with respect to time to form the signal pattern of target terrain.

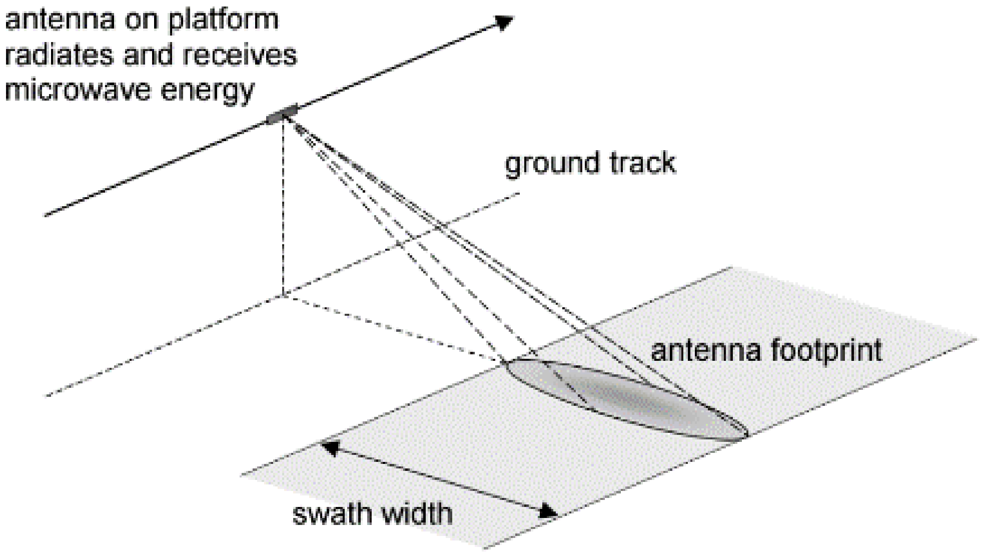

Figure 4.3: The figure shows the radar imaging geometry.

The pulse signal is commonly called ranging pulse and the rate at which they are repeated is called Pulse Repetition Frequency (PRF). The PRF is synchronized with the platform so that the strips of land are covered continuously, pulse by pulse.  This is visualized in fig 4.4 where large strips of terrain are covered with every successive pulse.

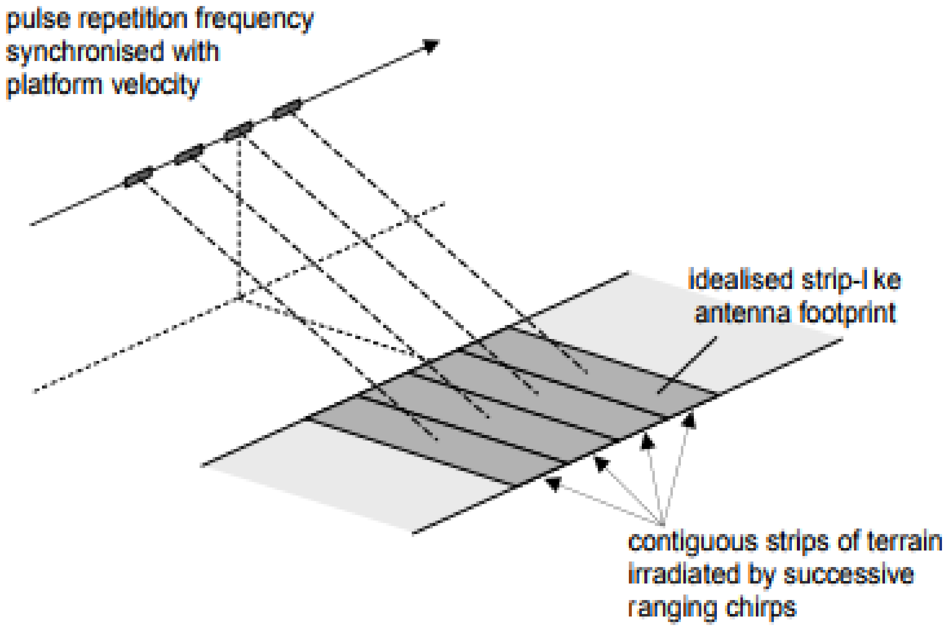

Figure 4.4: Successive ranging pulses are transmitted synchronously with platform velocity to cover most of the terrain

One of the major restrains for PRF is that if all echoes from a transmission are not returned before the next transmission range then ambiguity occurs, the data is corrupted, and distance of target is no longer accurate. This is prevented by restraining PRF with respect to slant range and velocity of the satellite. Therefore, the highest possible PRF is bound to the largest slant range (direct line from radar to a point on ground) of the system. The maximum usable PRF is further discussed in (Richards, 2009)

### *Radar Signal*

Most of Radar systems in remote sensing use monochromatic signals (Ferretti, 2014). A monochromatic signal is a sinusoidal signal at the central frequency.  This is evidenced as a sinusoidal arrangement of the E.M. field, i.e., when the signal is “frozen” in time the E.M. field will have constant sinusoidal pattern throughout. If the same experiment is conducted to a light bulb, i.e. observing the frozen E.M. field, we would see that none of the field will have any fixed relationship to the other within the beam. Since the radar sensor is coherent the beam follows a constant pattern. To achieve this constant transmitted signal the signal is modulated to carrier frequency, so the transmitted signal remains identical. This is also called modulation.

The returned signal (echo) is demodulated, i.e. the echo which is an analog signal is multiplied by the original carrier function and with a 90-degree shifted version of the signal (fig 4.5). Through demodulation and after filtering the real and imaginary part of the complex number of the respective pixel is obtained. This process is done by the satellite and the concept is explained in detail in (Ferretti, 2014)

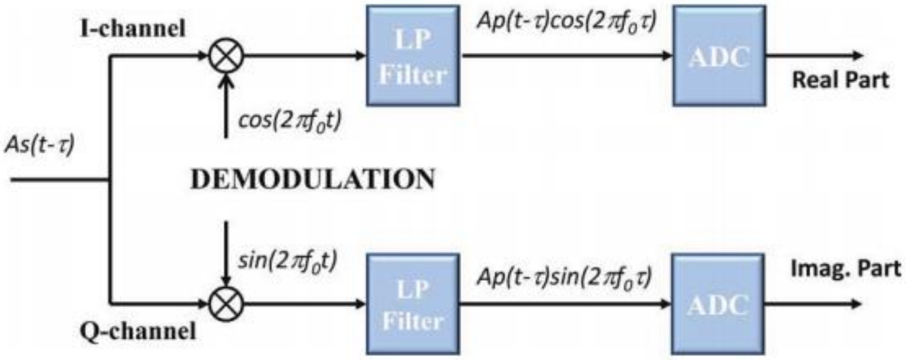

Figure 4.5: Simplified diagram of the radar receiver. Which shows the creation of real and imaginary part of the image from which the phase and amplitude are developed.

### *Radar Image*

The radar image is formed as follows. The moving satellite fires a burst of microwave signal at an angle from its side. When this signal makes contact with the surface part of the signal is lost and rest is scattered back. Since the signal is fired from a moving platform (e.g. satellite) at a slant angle the backscatter returns in delayed time with respect to the orthogonal direction of the satellite. This helps in locating the position of the target in the orthogonal direction. Since the platform will be firing the signal in bursts the intensity of the signal with respect to a target location will increase and decrease with successive bursts until the target leaves the footprint of the signal, this helps in determining the location of the target with respect to the satellite path. From the above we can find the signal with respect to each target location. The signal is converted from analog to digital by demodulating with respect to two channels which produce the real and imaginary part of the complex number. These details are then used to create the amplitude and phase of a radar image.

The radar imaging systems are divided into Real Aperture and Synthetic Aperture. Real aperture fires small bursts while synthetic aperture is capable of covering large area. For covering large area as such needed in landslide analysis synthetic aperture is most suitable.

## SAR

To understand how SAR is advantageous the resolution in Real Aperture is introduced first. The Real Aperture resolution in azimuth direction can be measured as (Thomas M. Lillesand, Ralph W. Kiefer 1989):

$$r_a = \frac{\lambda}{l_a} R_a \tag{3}$$

where

$r_a$ = Resolution in azimuth direction

$\lambda$ = Wavelength of signal

$l_a$ = Antenna length in azimuth direction

$R_a$ = Slant range distance or Distance to target

The above equation suggests that for a satellite flying at 1000km altitude with 3m long antenna and 3cm wavelength will have a Real Aperture resolution of 10km. For obtaining a resolution of 1m the satellite will need to either fly close to earth or increase the length of its antenna to impractical scales. To counter this, Carl (Carl, 1951) suggested the concept of synthetic aperture. He proposed that one can simulate a large antenna by predicting the reflected signals location, when the signal is launched at an angle. Using this concept, the length of antenna becomes the foot print of antenna. This would mean that the size of antenna can increase to a massive scale and resolution in range of meter is achieved. Then equation 3 for azimuth resolution becomes:

$$r_a = \frac{l_a}{2} \tag{4}$$

The above equation implies that synthetic aperture is more practical since good resolution images can be obtained with relative short antennas. The details of the derivation of equation (4) are reported in (Richards, 2009).

## InSAR

The previous sections discussed how radar imaging can cover large area with synthetic aperture. The sensor is also able to detect deformation in order of millimeter by combining, or interfering, signals from two antennas that are separated spatially or temporally. The radar signals from the two acquisitions will travel distance of $r_1$ and $r_2$ to antennas $A_1$ and $A_2$ respectively. The difference between $r_1$ and $r_2$ will result in the signal being out of phase by some phase difference ranging from 0 to $2\pi$ if the geometry of the interferometric baseline, i.e., the distance between the two antennas, is known. This distance is known to high degree of accuracy which helps to obtain the phase difference that is used to calculate the elevation of a point.

There are multiple ways for collecting Interferometric radar data. The basic approach is the *single-pass interferometry* in which a satellite carries two antennas, one antenna acts as both the transmitter and receiver, but the second antenna acts only as a receiver. The interferometric baseline is the distance between the antennae which result in low error when detecting the elevation of a target. The other type is the *repeat-pass interferometry* in which a satellite carries only one antenna which acts as both transmitter and receiver. To obtain the elevation of the target the satellite needs to travel two times over the target and to minimize the error the second pass must have a baseline less than 10 meters. From this definition, it seems that repeat-pass interferometry has high complications, but when the purpose of the satellite is to monitor a region like in the case of landslide investigation then this process becomes advantageous. Applications where InSAR is advantageous include measuring the glacier movement, the detection of moisture content in soil by obtaining the surface moisture and subsidence of a city due to pumping of water, among others.

## *InSAR Mathematical Background*

In this section InSAR concept is explained in mathematical terms for better explanation of advanced InSAR techniques in future. An SAR image contains information on the amplitude and phase of the reflected signal. The deformations estimation is based on the phase value. Mathematically phase value, Φ(P), of single acquisition of a pixel, P, having its coordinates in range and azimuth can be written as (Ferretti, 2014)

$$\Phi(P) = \varphi + \frac{4\pi}{\lambda} r + \alpha + \nu \quad (5)$$

where:

(i) "$\varphi$" is the reflectivity phase. This factor takes into consideration that total reflection does not take place and scattering occurs due to target/location;

(ii) "$\frac{4\pi}{\lambda}$"is the location of "electromagnetic barycenter "of all elementary scatterers, λ being the wavelength of the signal;

(iii) "r" is the sensor to target distance;

(iv) "$\alpha$"is the effect of the atmosphere on the electromagnetic wave. The quality of the final result depends on this factor; and

(v) "$\nu$" depends on noise or more importantly thermal noise of the radar system.

The phase value of single SAR image has no use because the contribution of the different phases cannot be separated, and all the wrapped phase values seem to be unrelated. This is where the concept of SAR Interferometry comes in by introducing the difference in the phase values of each pixel "P" from two acquisitions. Equation (5) becomes

$$\Delta\Phi(P) = \Delta\varphi + \frac{4\pi}{\lambda}\Delta r + \Delta\alpha + \Delta\nu \tag{6}$$

An interferogram is developed by calculating the phase difference of individual pixels. In case of *single pass interferometry* all the parameters in equation (6) other than $\Delta r$ turn to zero and Equation (6) turns to

$$\Delta\Phi(P) = \frac{4\pi}{\lambda}\Delta r \tag{7}$$

But in other cases, most of the parameters are still present and in some cases additional parameters appear in $\Delta\varphi$ and $\Delta\alpha$ of equation (6). Different procedures are performed to mitigate the effect of errors in the phase of an image. These include choosing existing DEMs to predict the phase value and reducing the perpendicular baseline (see appendix for definition). DInSAR is a method that removes topographic phase which is the phase value due to the existing topography to generate the required phase information.

## DInSAR

Differential SAR Interferometry is an interferometric technique to analyze and quantify the surface movement. This is done by removing the effect of topography in the area of interest. This process can be better understood by progressing from the phase equation (6). By removing the topographic phase, the phase of surface deformation is clearly visible

$$\Delta\Phi_D = \Delta\Phi(P) - \Phi_{topo} = \Phi_{displacement} \tag{7}$$

Where

$\Delta\Phi_D$ Is the Differential phase

$\Phi_{topo}$ Is the simulated topographic component (The topographic component is simulated from existing topographic data)

The above equation is used to remove the effect of topographic related phase components. The removal of topographic phase is necessary to estimate the change in landmass or displacement of landmass. This is done by using an existing Digital Elevation Map (DEM) of the area of interest from previous acquisitions and generating a synthetic interferogram, which is then subtracted from the interferogram generated by equation (6). This means that the accuracy of the DInSAR depends on the existing DEM, however the DEM error can be estimated and compensated as mentioned in (Alessandro Ferretti A. M.-G., 2007). Due to accurate GPS receivers onboard satellites, DEM errors are close to non-existent. They generally exist in areas where the topography changes frequently and it is tough to get new and accurate DEM's.

### *SAR Satellite Wavelength*

Radar satellites are divided based on the wavelength of their signal (UNAVCO, 2015). The X-Band has the shortest wavelength and is around 3cm and is used by the military for maritime monitoring. The L-Band has the highest wavelength and is used for monitoring activity in high vegetation. Fig (4.6) summarizes different satellite missions, their duration and their wavelength. For the analysis in this work, Sentinel-1 satellite data is used Sentinel-1 is a C- band satellite implying a wavelength between 4cm – 8cm. C-band wavelength is used for monitoring in cities. Different wavelengths behave in unique manner when they react with the surface. In general, the shorter the wavelength the better it is to detect ground motion. However, shorter wavelength has its disadvantages in obtaining coherent images(Agram 2013).

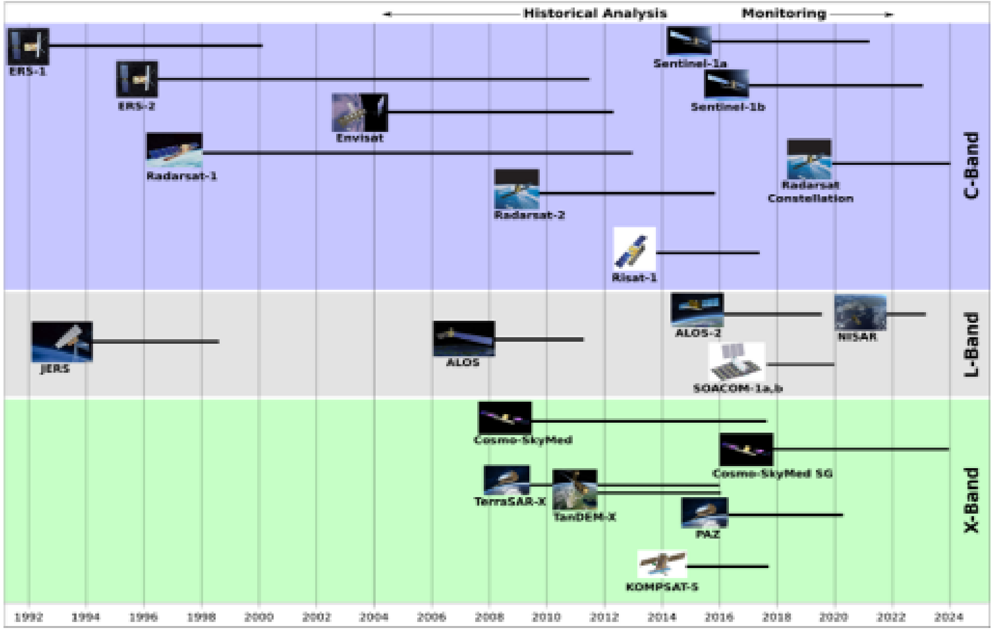

Figure 4.6: This image shows a chart of present and past SAR satellites.

Radar penetration is graphically depicted in Fig (4.7) and outlined next, in view of effects of vegetation, dry soil conditions, and ice.

Vegetation

In general, L-band signals can penetrate leaves and trees, C-band signals can penetrate through minor vegetation, while X-band signals are reflected by leaves. Therefore, L band sensor is ideal to measure displacements in areas with high vegetation landscape while C and X bands are useful for measuring displacement in urban landscape.

Dry soil conditions:

For dry soil conditions, the L-band signal penetrates dry soil and is ideal for measuring soil moisture content, while the C-band partially penetrates dry soil and X-band is reflected by the surface roughness.

Ice

When ice covers the surface of the target, the L band signal can penetrate the ice layer completely.  The C-band signal partially penetrates the ice; however, the X-band cannot penetrate the ice layer and is ideal for measuring glacier displacements

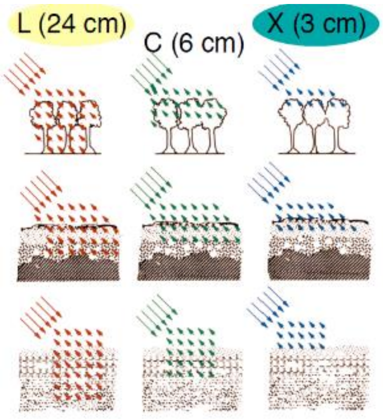

Figure 4.7: This image shows the microwave penetration of different SAR sensors(Agram 2013).

# Chapter 5

# DInSAR Implementation

To apply the DInSAR technique to detect landslides two open sourced programs are used, i.e., SNAP and SNAPHU

## *SNAP*

*SNAP* is a part of Scientific Toolbox Exploitation Platform (STEP) and stands for Sentinel Application Platform, which is jointly developed by ESA with help from Brockmann Consult (Brockmann Consult, 2017) and Array systems computing (array systems, 2017). SNAP replaced NEST in late 2014 as primary remote sensing software developed by European Space Agency (ESA).

Since the program is open source the community is active in *forum.step.esa.int* where all the questions related to the program are discussed. Some of the developers who moderate the forum also consider the suggestions that appear in the forum to improve the program. Unlike other SAR programs SNAP shifted from code based to interface based to make the program more accessible.

## *SNAPHU*

Statistical Cost, Network-Flow Algorithm for Phase Unwrapping is developed in standard by Dr Chen and Dr Zebker (C. W. Chen and H. A. Zebker 2002). SNAPHU is a

Linux based program which is used to perform 2-D phase unwrapping. For phase unwrapping SNAPHU is the most reliable tool as it can perform a lot of computationally expensive problems.

The data obtained from Sentinel-1 is processed using SNAP following the steps mentioned in figure (5.1) and discussed following. The steps mentioned below are repeated for each data set and the results are studied separately (Veci, 2016).

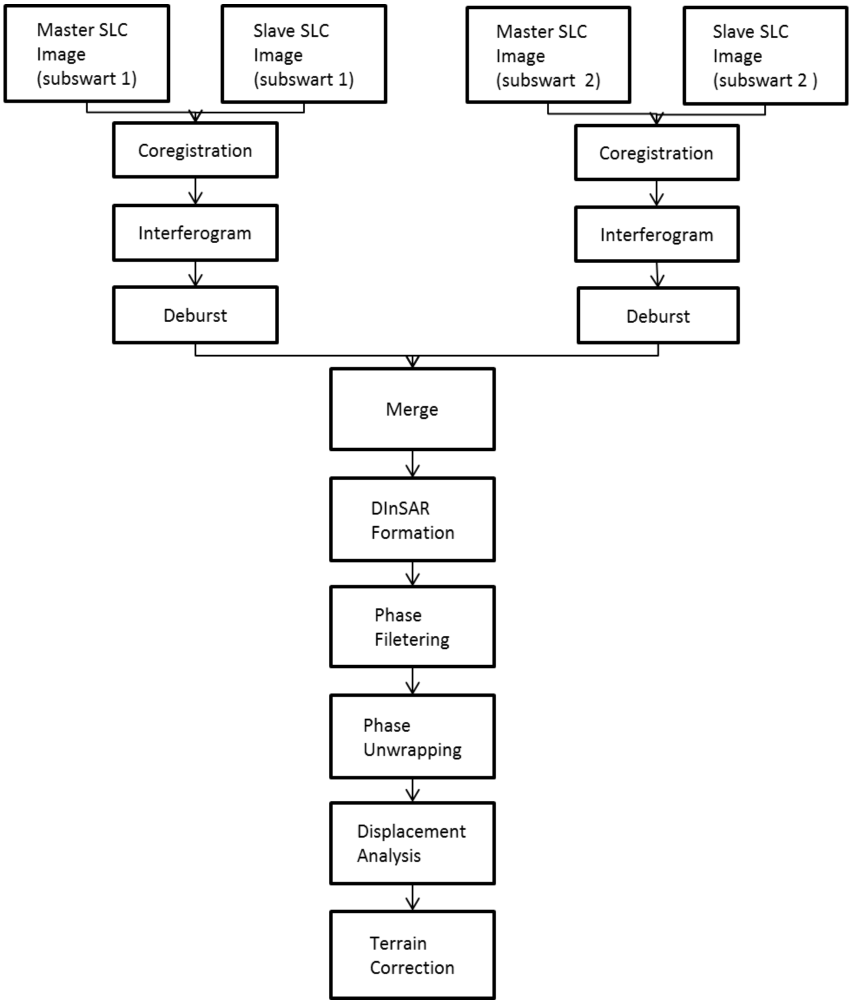

Figure 5.1: This image shows the flowchart followed for DInSAR analysis.

### Step-1 Coregistration

Coregistration is the critical step in which pixel to pixel matching is performed on two acquisitions so that accurate phase difference can be calculated in order to increase coherence and reduce the noise. To coregister the two images one image is chosen as the master and other is the slave. The slave image is superimposed on the master, and, typically the older image is chosen as the master as this helps in detection of deformation in later stages. Orbit files are applied to each acquisition and resampling is done to complete the coregistration process. The orbit files provide accurate position and velocity of the satellite for the time of acquisition. For this study TOPSAR (appendix A) data is used which is split into 3 parts called sub swaths and the sub swath with the target image is processed. This is done to prevent the processing from becoming computationally expensive. During the splitting process, the polarization (appendix A) of the images is also chosen. The polarization of master and slave must be same to prevent errors.

The above steps can be performed in SNAP individually or in single step using the S-1 TOPS coregistration option.

### Step-2 Interferometric Process.

In the coregistration step the pixel values are aligned. To develop an interferogram, the phase value of the slave is removed from the master as per equation (6). However, equation (6) does not generate accurate interferogram as it does not consider flat earth phase. In reality, due to numerous reasons such as the earth being an irregular ellipsoid, and the satellite tilt, additional phase element is present during the generation of the interferogram, introducing, thus, an error in the interferometric phase. This error is called flat-earth phase. The flat earth phase can be computed from the perpendicular baseline (see appendix A for definition) and removed to generate a better interferogram. In SNAP the flat earth phase is removed during the interferogram formation.

### Step-3 Deburst

This step is performed exclusively to acquisitions taken through TOPS (see appendix A for definition) technique. This is because in TOPS the satellite covers long strips of area that are separated by demarcation zones. These demarcation zones contain random values and need to be removed through debursting so that these zones will not affect future processing. Deburst is done in SNAP using the TOPS-DEBURST option.

### Step-4 Merge

This step is also performed almost exclusively to acquisitions taken through the TOPS technique. This step is performed if the target area is located in more than one sub swath. All the above-mentioned steps are repeated to each sub swath and they are merged using the TOPS merge option in SNAP

### Step-5 Topographic Phase Removal

Topographic phase removal is used to generate the DInSAR phase. The topographic phase is estimated from existing DEM (see appendix A). If the target area is not located near the poles the existing DEM used is SRTM (appendix A). By removing the topographic phase, the resulting phase will have the ground motion phase visible, although additional filtering needs to be done for better image resolution. In SNAP multiple DEM options are available to perform this step and they must be considered based on the location and satellite used for acquisition. Some locations are not covered by existing DEMs this is because of the satellite paths and the targets geo coordinates need to be compared before choosing the right DEM.

## Step-6 Phase Filtering

This step is optional but is recommended as this step reduces the noise, helps in product visualization and increases the accuracy of the phase unwrapping process (appendix A). For phase filtering the algorithm developed by R.M Goldstein and C.L Werner (Goldstein, 1998) is used as this method produces best results for Geophysical applications. In SNAP a separate option is available to perform Goldstein phase filtering.

## Step-7 Phase Unwrapping

From step-6 the ground motion can be observed but actual displacement cannot be measured. To develop the displacement maps the wrapped phase should be converted to continuous form. This process is performed in SNAPHU a lynux based software. The result from step-6 is exported to SNAPHU where after the unwrapping is completed the finished product is imported back to SNAP to perform the final part of test.

Unwrapping is performed by using the command *“$ snaphu -f snapu.config (file name).img*” in the terminal.

## Step-8 Displacement Analysis

The unwrapped phase is imported back to SNAP and converted to displacement. The displacement generated is the displacement in the direction of line of sight of the satellite. In SNAP the unwrapped phase can directly be converted using the phase to displacement option.

### Step-9 Terrain Correction

Terrain Correction is a necessary step to remove the misleading influence of topography on backscatter values and satellite tilt. These distortions are removed by using the meta data available with the reading or by using external precise orbit with reference DEM data to derive precise geolocation information. This correction can be performed after any step, but after terrain correction no additional processing can be done. This step is performed on data that needs to be exported to google earth for observations.

This step is performed in SNAP using the Range Doppler Terrain Correction operator (Appendix A).

# Chapter 6

# DInSAR Showcase Studies

Three areas have been selected to demonstrate the implementation of the DInSAR methodology, i.e., Mount Etna in Italy, Highway 1 in California USA and Anargyroi lignite quarry in Greece. In all three areas massive landslides have occurred in the last two years due to different triggering mechanisms.

## Satellite information

For landslide analysis data from Sentinel-1mission is used. Sentinel-1 is a polar orbiting radar mission which has 2 satellites Sentinel-1A and Sentinel-1B. They were both launched respectively on 3 April 2014 and 25 April 2016 using Soyuz rocket from European spaceport in French Guiana. Each Sentinel-1 satellite passes a target area every 12 day and would cover the entire world mass. The satellite is expected to transmit data for 7 years at minimum and have fuel for 12 years (ESA, 2016).

## Study Areas Description

### *Etna*

Mount Etna is an active volcano covering an area of 459mi$^2$ which had the most recent eruption on 16 March 2017. The volcano is located in Sicily, Italy. Sentinel 1 data used to analyze the effect of Etna eruption is acquired on February 2, 2017, March 3, 2017, March 14, 2017, and March 26, 2017. The aim of this analysis is to see the effect of the volcano on the topography and to detect any possible landslides that are developed because of it.

### *California Highway 1*

California State Route 1 is a major highway along the pacific coastline. The route is 655.8miles and is the longest state route. A major mudslide occurred on May 20th 2017 causing major disruption to traffic. The global coordinates of the landslides are covered by Latitude 35.8709 Longitude -121.4382 and Latitude 35.8592 Longitude -121.4225. For analysis, we will use Sentinel 1 data of the area, acquired on April 25,2017, May 07,2017, May 19,2017, and May 31,2017. The aim of this analysis is to see if the landslide can be predicted by using DInSAR technique.

### *Anargyroi Greece*

Anargyroi village is located near a lignite mine which was affected by a landslide on June 10th, 2017. The landslide is induced by mining and triggered by the collapse of an open case lignite mine. The citizens of the village were evacuated but the village was destroyed due to landslide. The global coordinates of the landslide activity are covered by Latitude 40.6108 Longitude 21.5929 and Latitude 40.5941 Longitude 21.6311. For analysis, we will use Sentinel 1 data of the area, acquired on May 17,2017, May 29,2017, June 10,2017, and June 22,2017. The aim of this analysis is to see if this landslide can be predicted using InSAR technique.

*Dataset overview*

Sentinel-1 mission uses C-band imaging radar with 4 imaging modes and coverage up to 400km. It provides dual polarization capabilities with short revisit times (12 days). The datasets are named in the form of fig (6.1). For DInSAR, Single Look Complex(SLC) data type is used (ESA, 2017)

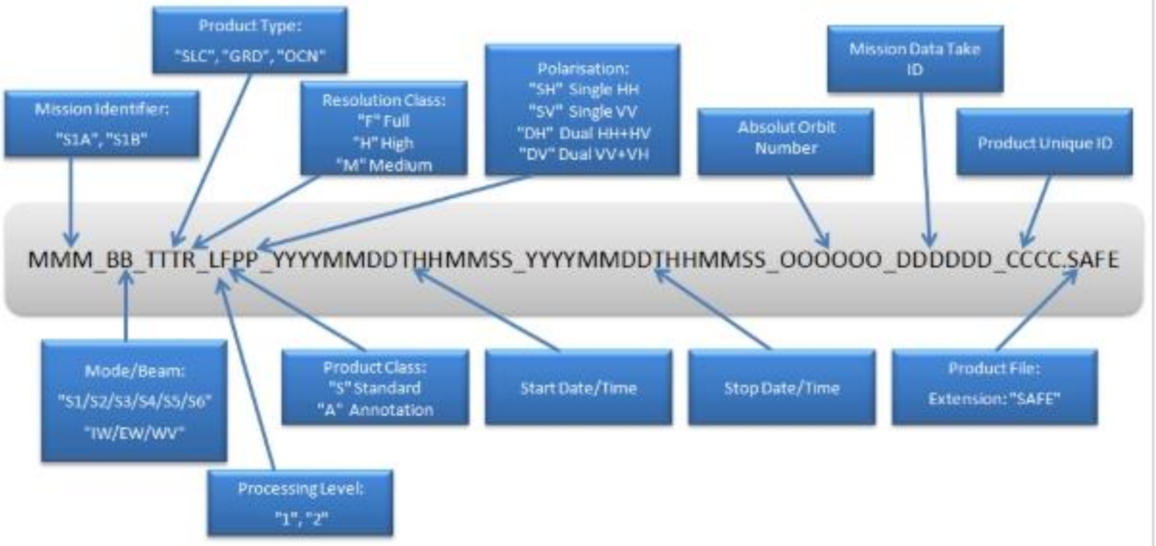

Figure 6.1: This image shows the significance of each part of the sentinel-1 dataset

Datasets

For DInSAR analysis SLC type acquisitions are used. Single Look Complex (SLC)images have focused SAR data and the pixels are spaced equally in azimuth direction and in slant range. The data is represented as complex numbers containing both phase and amplitude. SLC products are used for applications where the full bandwidth and phase information are required (AIRBUS defence and space, 2014).

*ETNA*

S1A_IW_SLC__1SDV_20170218T165557_20170218T165624_015341_01927E_40B5.SAFE

S1A_IW_SLC__1SDV_20170302T165557_20170302T165624_015516_0197CF_B591.SAFE

S1A_IW_SLC__1SDV_20170314T165558_20170314T165625_015691_019D20_0A0A.SAFE

S1A_IW_SLC__1SDV_20170326T165558_20170326T165625_015866_01A24E_E6CA.SAFE

*GREECE*

S1A_IW_SLC__1SDV_20170517T162401_20170517T162429_016624_01B94C_BF9F.SAFE

S1A_IW_SLC__1SDV_20170529T162353_20170529T162421_016799_01BEB0_92A1.SAFE

S1A_IW_SLC__1SDV_20170610T162354_20170610T162422_016974_01C41E_955A.SAFE

S1A_IW_SLC__1SDV_20170622T162355_20170622T162423_017149_01C979_27A9.SAFE

*CALIFORNIA*

S1B_IW_SLC__1SDV_20170425T020606_20170425T020633_005311_0094E3_4593.SAFE

S1B_IW_SLC__1SDV_20170507T020607_20170507T020634_005486_0099D1_B25E.SAFE

S1B_IW_SLC__1SDV_20170519T020608_20170519T020635_005661_009EA1_7930.SAFE

S1B_IW_SLC__1SDV_20170531T020608_20170531T020635_005836_00A3AE_1AA5.SAFE

## DInSAR Application in ETNA

The following are results from steps performed to obtain DInSAR results

- Step 1 corregistration: The fig (6.2) shows the intensity part of Etna datasets 3, 4 and subset 2

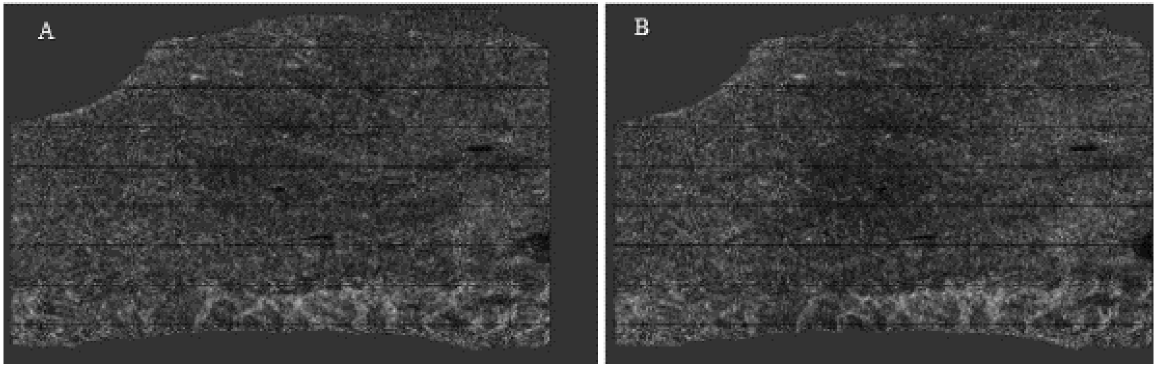

Figure 6.2: Image A was taken on 14 march and image B was taken on 26th march

- Step 2 Inteferogram generation: In fig (6.3) the interferogram is shown which is created from coregistered image from fig 6.2

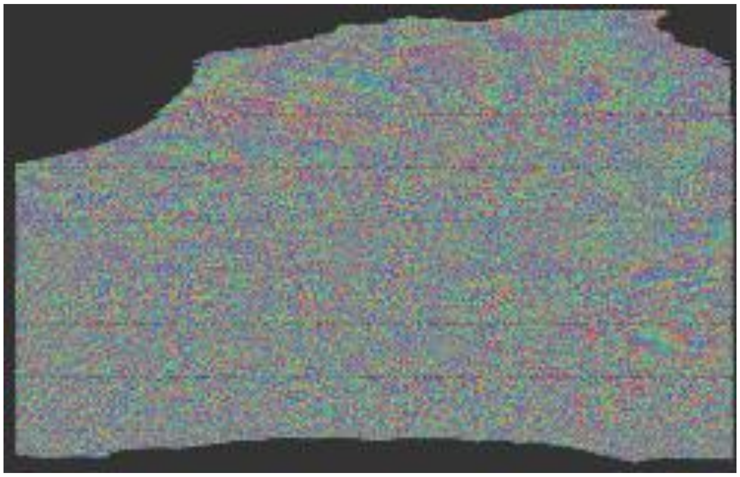

Figure 6.3: image shows a typical interferogram before any filtering is done, the Demarcation zones are visible.

- Step 3 Deburst: In fig (6.4) the interferogram is shown after the deburst where the demarcation zones are removed.

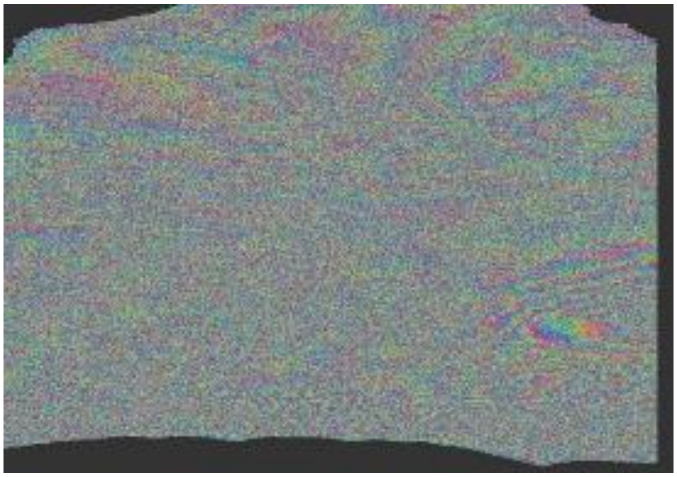

Figure 6.4: The image shows an interferogram in which the demarcation zones are removed.

- Step 4 Merge: In the experiment, the volcano Etna is located in between subset 1 and subset 2. In fig (6.5) shows interferogram after the subset 1 and subset 2 are merged.

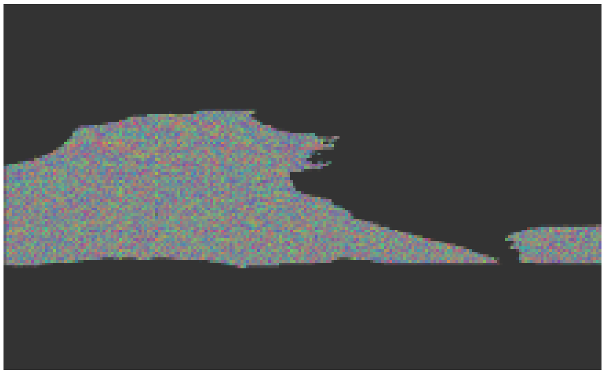

Figure 6.5: The image shows the interferogram after merging 2 subsets.

- Step 5 Topographic phase removal: In fig (6.6) the result from the topographic phase removal is shown.

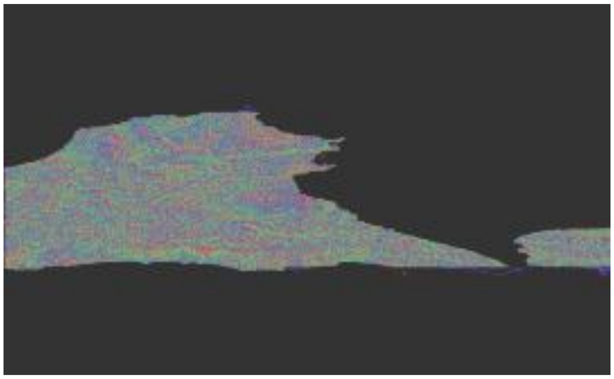

Figure 6.6: In This image, the topographic phase has been removed, although the displacement phase is visible significant noise is still available.

- Step 6 Phase filtering: Only volcano part of the fig (6.6) is processed as processing the whole would be computationally expensive. In fig (6.7) the result from Goldstein phase filtering is shown.

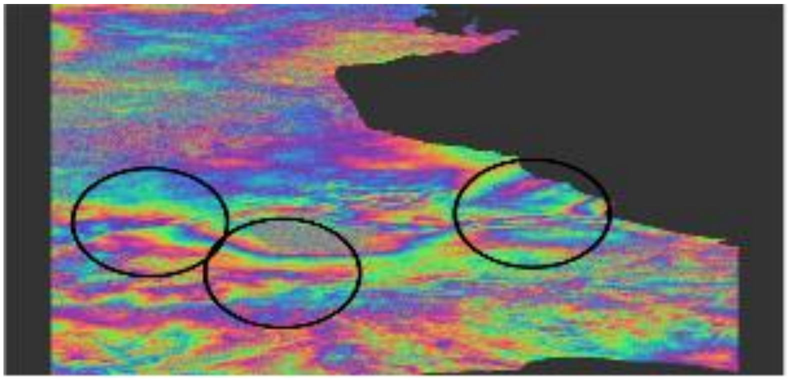

Figure 6.7: In this image, the displacement phase is clearly visible and are highlighted.

- Step 7 Phase unwrapping: This step is performed in SNAPHU and cannot be pictorially represented
- Step 8 Displacement analysis: In Fig (6.8) the result from displacement analysis is shown.

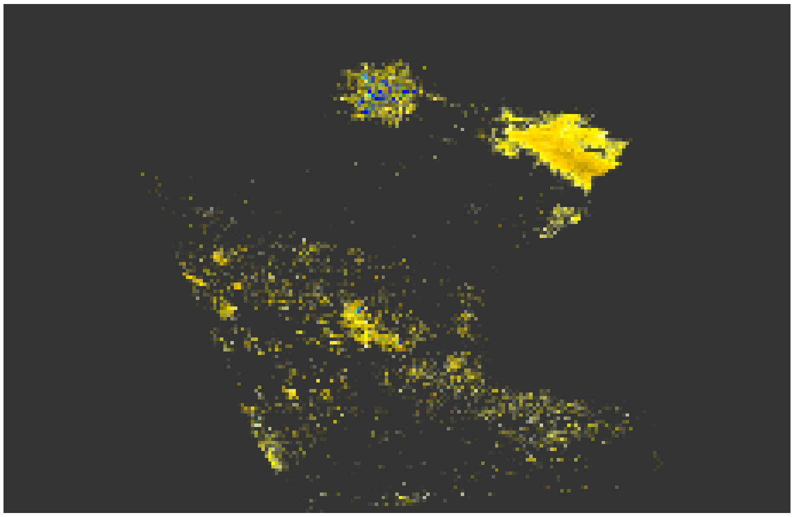

Figure 6.8: The image shows the displacement in the direction of satellite line of sight.

- Step 9 Terrain Correction: In Fig (5.9) the image after terrain correction is shown.

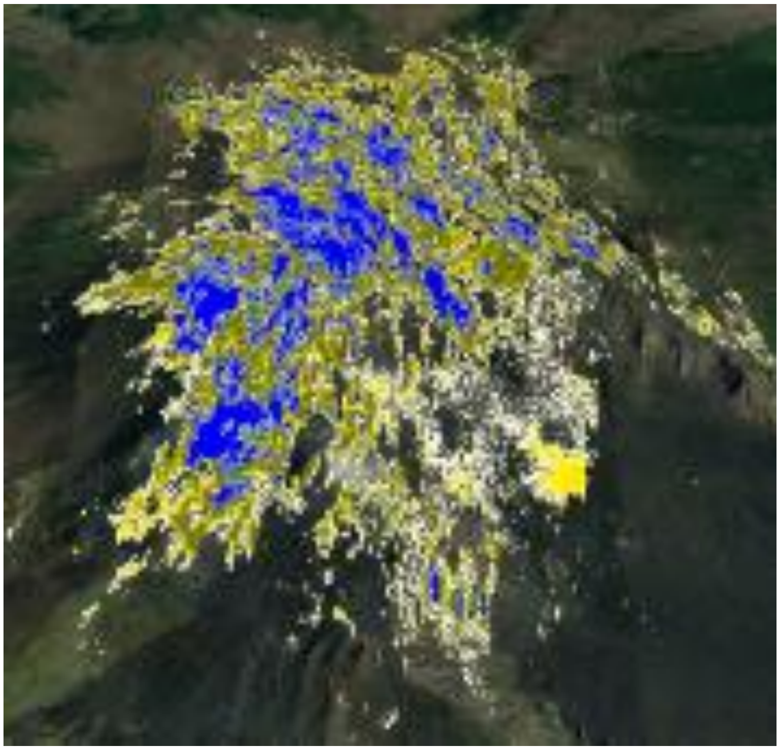

Figure 6.9: In this image, the displacement map is super imposed on google earth file for better understanding of the displacement.

# Chapter 7

# Results and Discussion

### *Mount Etna*

DInSAR analysis is performed using SRTM DEM as reference to develop phase maps of the area. Total of 3 interferogram phase, coherence and subsequent displacement maps are shown to analyze the effect of volcano to generate landslides in the region. The coherence is high in all 3 cases due to the fact that this is a volcanic region with minimum vegetation.  Fig (7.1) shows Mount Etna taken on June 5,2014 by Landsat mission. All images have been terrain corrected and exported to google earth for easier understanding

Figure 7.1: This is Mount Etna observed through the visual spectrum. This image shows the target area to be analyzed.

Test 1

For this test acquisitions taken on February 18,2017 and March 02, 2017 are analyzed. Fig (7.2) shows the phase reading of the region. From the image, we can see that there is no slope instability. The minor phase contours around the decolor zone suggest minor uplift in the crust.

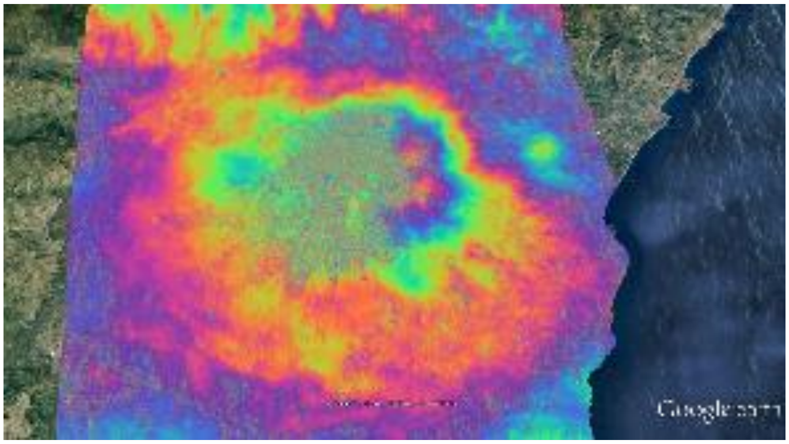

Figure 7.2: The image describes the phase properties of Mount Etna and does not have any significant phase variations which signify slope instability.

Fig (7.3) shows the coherence map of the region. From the coherence map we can see that other than near the center, the image has consistent high signal to noise ratio. The center has low coherence due shadowing.

Figure 7.3: The black region in the center describes the low signal strength and the whitish grey surrounding signifies high signal to noise ratio signifying better phase reading in this region.

Fig (7.4) shows the displacement analysis map of the region. The region with high subsidence(blue) cannot be considered as this region is under the poor coherence

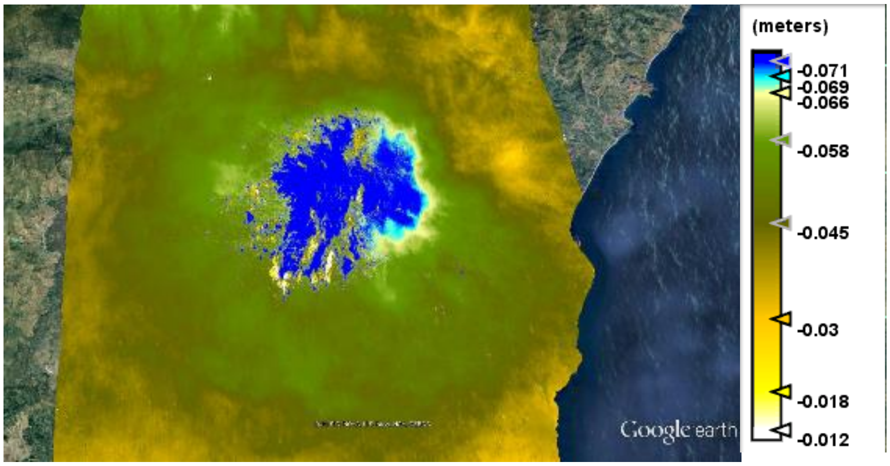

Figure 7.4: The above image shows minor subsidence around the image center although this reading can be considered calibration error.

Test 2

For this test the acquisitions taken on March 02,2017 and March 14,2017 are analyzed.

Fig (7.5) shows the phase of the region and no major slope instability can be seen in the image

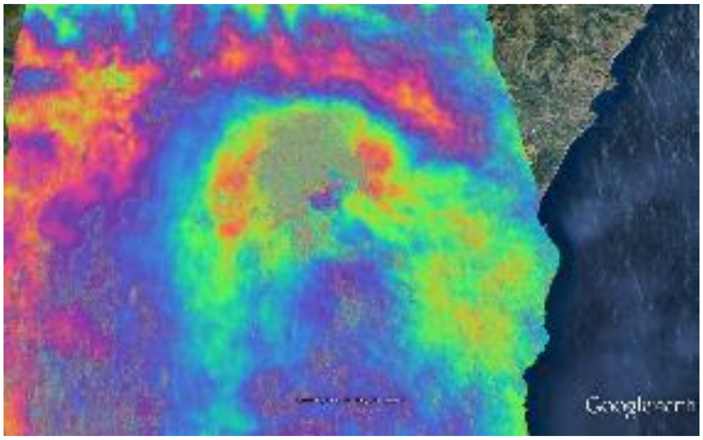

Figure 7.5: This image does not show any significant phase variation that confirm slope instabilities in the region.

Fig (7.6) shows the coherence map of the region and from the map we can see that the center of the mount has poor coherence(black).

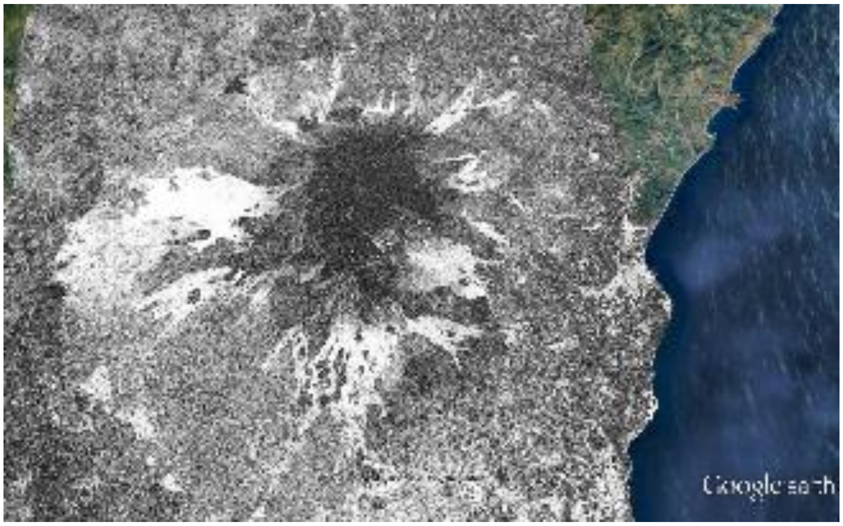

Figure 7.6: The black region in the center describes the low signal strength and the whitish grey surrounding signifies high signal to noise ratio signifying better phase reading in this region.

Fig (7.7) shows the displacement analysis map of the region. The constant subsidence cannot be considered as this could be due to calibration error or presence of minor vegetation.

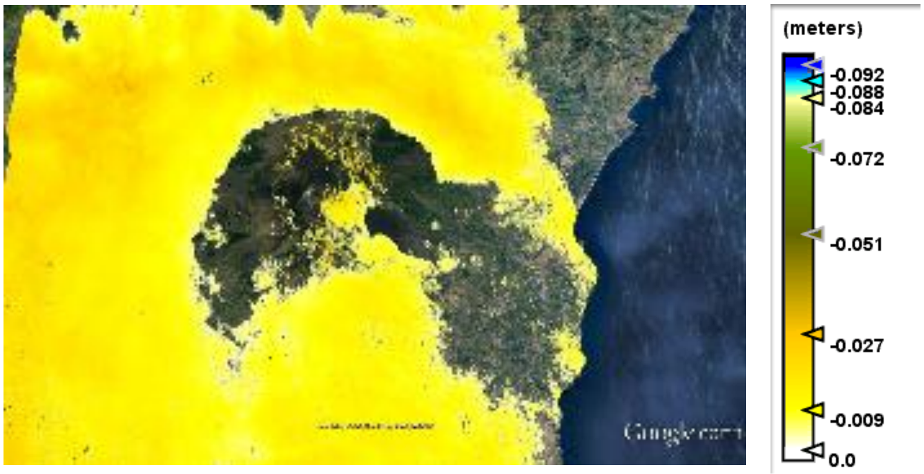

Figure 7.7: The constant subsidence visible in the image is not considered as this reading can be due to calibration error or due to minor vegetation.

Test 3

For this test acquisitions taken on March 14,2017 and March 26,2017 are analyzed.

Fig (7.8) shows the phase of the region with significant phase activity the color changing contours signify the slope instability and possible landslide activity in the region.

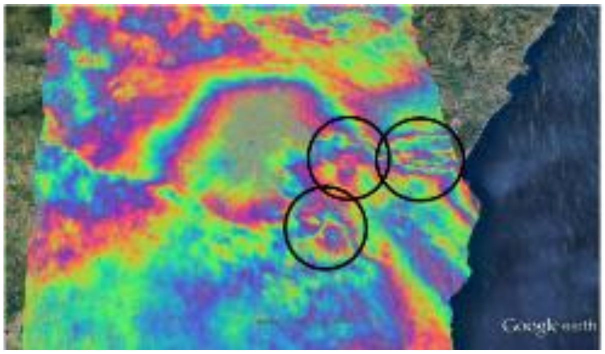

Figure 7.8: The high lightened region signifies slope instability and possible landslide activity.

Fig (7.9) shows the coherence map of the region and from the map we can see that the center of the mount has poor coherence (black). This signifies that other than the poor coherence area we can consider the rest of the area for our observations.

Figure 7.9: Shows the coherence map of the region and from the map we can see that the center of the mount has poor coherence(black) because of this the poor coherence part is not considered for our discussion.

Fig (7.10) shows the displacement analysis map of the region. The displacement map covers the volcanic event. Other than the zone with poor coherence there does not seem to be any activity in the region this is considering the minor subsidence is due to calibration error and vegetation.

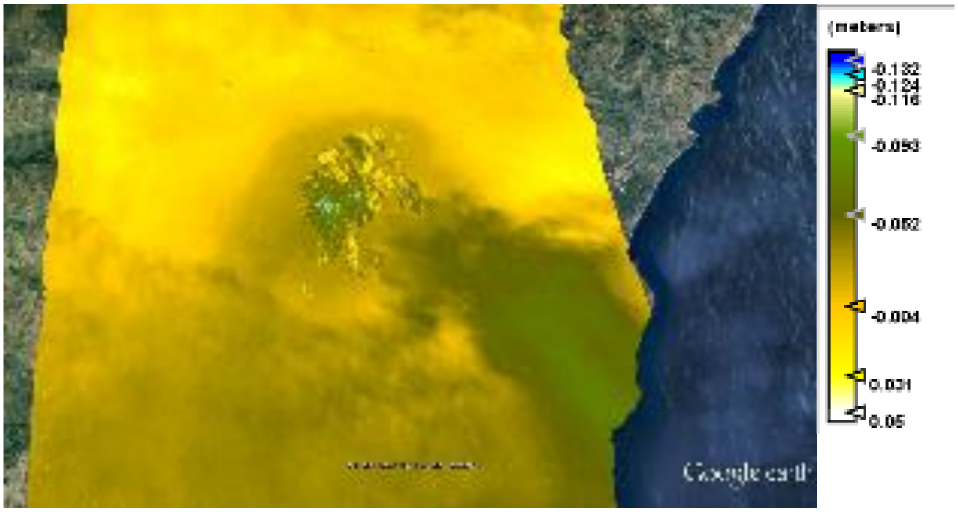

Figure 7.10: The image shows minimum displacement activity due to the volcanic action.

*Discussion*

Considering the 3 analysis we can observe that the images have high coherence. High coherence images generate accurate interferograms from which ground motion can be easily detected. In Fig (7.3,7.6,7.9) we can see that the center of the Etna crate has high noise, and this is due to the principle of shadowing and layover. Where the signal cannot return back to the satellite, because it is prevented from returning by the crater walls.

The phase from test-1 and test 2 show that there is low seismic activity in the region. Test 3 which covers the eruption shows multiple fringes (highlighted) which represents the slope instability and possible landslide activity.

The coherence map represents the signal to noise ratio, with white being 1 i.e. full signal strength and black being 0 i.e. meaning no backscattering signal. The coherence in all three tests is consistent with the slope of the mount having high coherence and the volcanic crater having low to nonexistent coherence. This is also due to the direction of the satellite flight path and can change if the satellite path is different. The path of satellite in all 3 cases is ascending that means the satellite is travelling from south to north.

The displacement maps show the displacement in the direction of satellite line of sight. The -ve sign represents subsidence. The displacement observed in each test is the displacement taking place between the two acquisitions. Finally, the accuracy of the displacement maps is not definitive and must be correlated with in-situ readings to calibrate the displacement data and estimate the error due to vegetation. It should also be noted that the phase change associated with landslide activity that have been highlighted in fig (7.8) are not visible in displacement map fig (7.10). Additional phase elements might also effect the displacement maps that have not been removed in the analysis stage.

### *California Highway 1*

DInSAR analysis is performed using SRTM DEM as reference to develop phase maps of the area. Total of 3 interferogram phase, coherence maps are shown to detect changes that would signal landslide activity. The displacement map of the area is not developed due to the process being computationally expensive to develop. Fig (7.11) shows the highway before and Fig (7.12) after the landslide event has taken place, both the images have been taken by Landsat.

Figure 7.11: This image was taken before the landslide occurred by Landsat satellite.

Figure 7.12: This image shows effect of landslide on the highway and is taken by Landsat satellite.

Test 1

For this test acquisitions taken on April 25,2017 and May 07,2017 are analyzed.

Fig (7.13) shows the phase of the target area. From the image, we can see that there is some phase activity in the slope where the landslide is expected to take place. This phase activity (highlighted) is different from the phase activity visible when slope instability takes place.

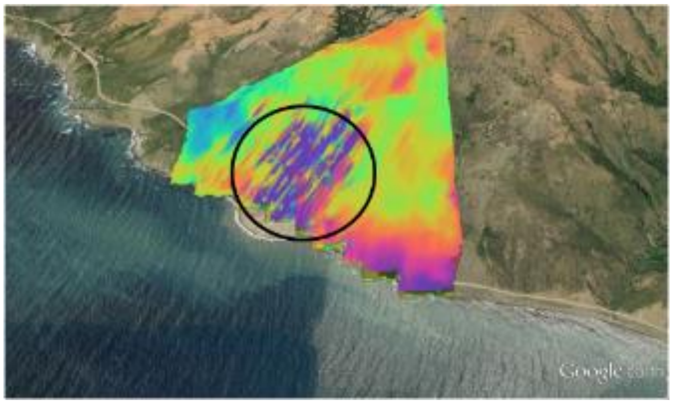

Figure 7.13: the highlighted part shows some phase disturbance which are not related to slope movement as phase corresponding to slope movement has distinct contour like pattern.

Fig (7.14) shows the coherence map of the target area. The signal to noise ratio in the region is good with no particular parts that show very bad coherence

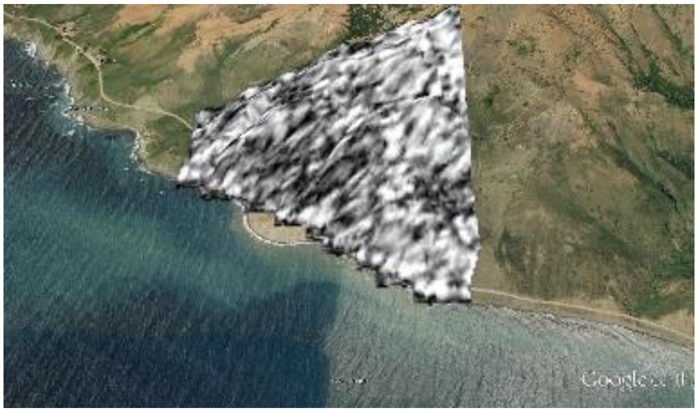

Figure 7.14: The image shows good coherence with more grey and white area signifying good signal strength.

Test 2

For this test acquisitions taken on May 07,2017 and May 19,2017 are analyzed.

Fig (7.15) shows the phase activity which is consistent with what was observed in fig (7.14).

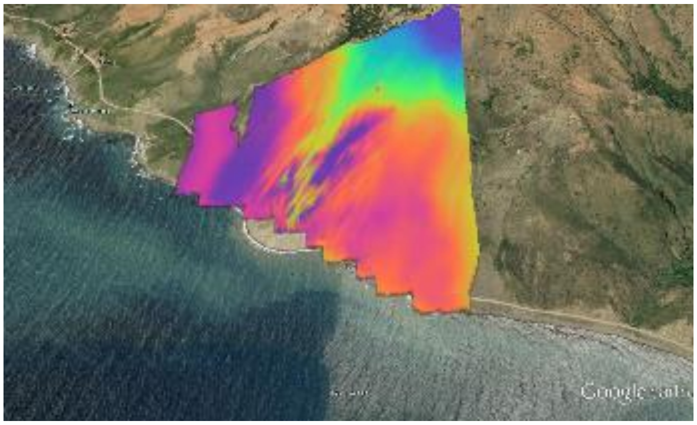

Figure 7.15: The image shows good phase reading that is visible with the location where the landslide is to take place having some activity.

Fig (7.16) shows the coherence map of the region. This acquisition has higher signal to noise ratio as compared to fig (7.15) this is visible with higher presence of white region.

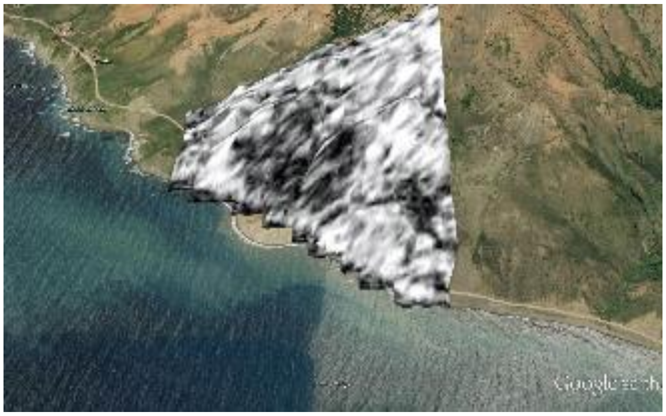

Figure 7.16: This image shows there is high white color presence which signifies good signal to noise ratio.

Test 3

For this test acquisitions taken on May 19,2017 and May 31,2017 are analyzed.

Fig (7.17) shows the phase of the region. In the image, the landslide incident is clearly seen in the phase with the flow pattern covering the area

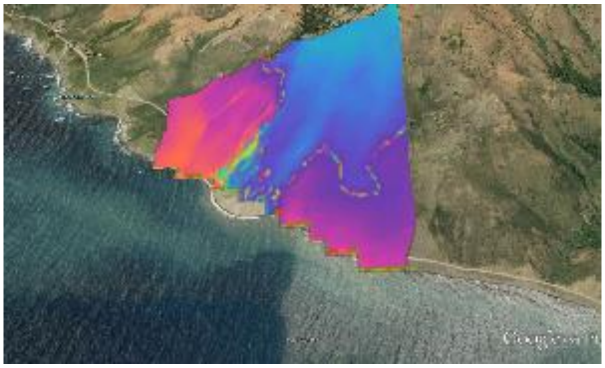

Figure 7.17: The landslide incident is clearly seen in the phase image with the flow covering the target region.

Fig (7.18) shows the coherence map of the region. In the image, there is low coherence in the region where the landslide has taken place.

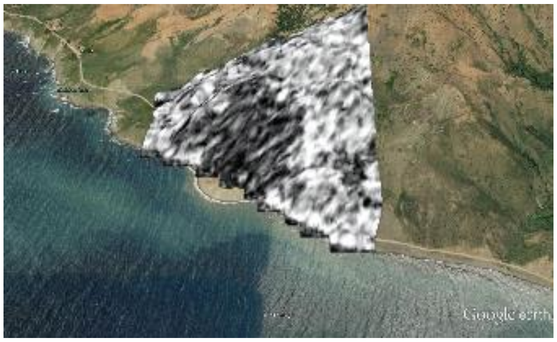

Figure 7.18: The image shows poor signal to noise ratio in the area where the landslide has taken place but the area surrounding it has good signal to noise ratio.

### *Discussion*

The coherence maps of the target region suggest that most of region has good coherence with average coherence being between 0.44 to 0.48 for the 3 cases.

The phase map from test 1 shows there is some form of abnormality near the target region. This abnormality is not caused by layering or shadow effect. This can be confirmed from the path of satellite (Ascending). The change in phase can be due to presence of high water content in the soil. News report suggest that the landslide is a type of mudslide and the prominent reason for a mudslide is the water content in soil. This reason is also reinforced by the fact that the radar waves behave differently when they interact with wet and dry soil.

The phase map from test 2 also reinforces the observations from test 1. The phase from test 3 which covers the incident shows the landslide taking place.

Although displacement maps were not available for this test the phase maps were able to provide a possible landslide recognition opportunity. Further tests must be conducted in similar conditions to confirm these findings.

### *Anargyroi Greece*

DInSAR analysis is performed using SRTM DEM (appendix) as reference to develop phase maps of the area. Total of 3 interferogram phase, coherence maps and subsequent deformation maps are shown to detect changes that would signal landslide activity. Fig (7.19) shows the area near Anargyroi before landslide and Fig (7.20) shows the area after the landslide has taken place, the picture has been taken by Landsat.

Figure 7.19: The above image shows the lignite mine operational and before the landslide event.

Figure 7.20: The above image shows the area after the collapse of the mine due to landslide.

Test 1

For this test acquisitions taken on May 17,2017 and May 29,2017 are analyzed.

Fig (7.21) shows the phase of the region. Significant part of image is discolored due to poor coherence.

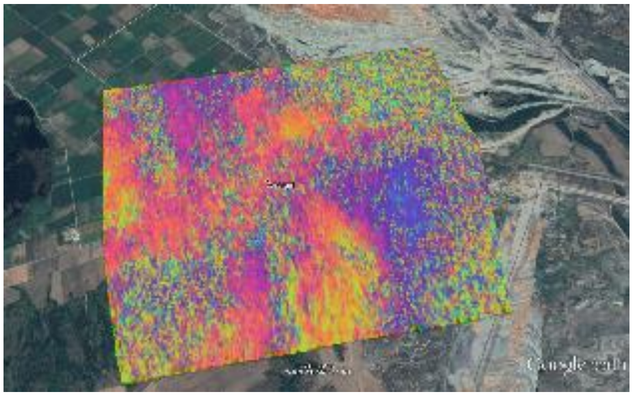

Figure 7.21: most of the image shows low phase visibility.

Fig (7.22) shows the coherence map of the region. From the map, we can see that significant portion of the image is low in coherence

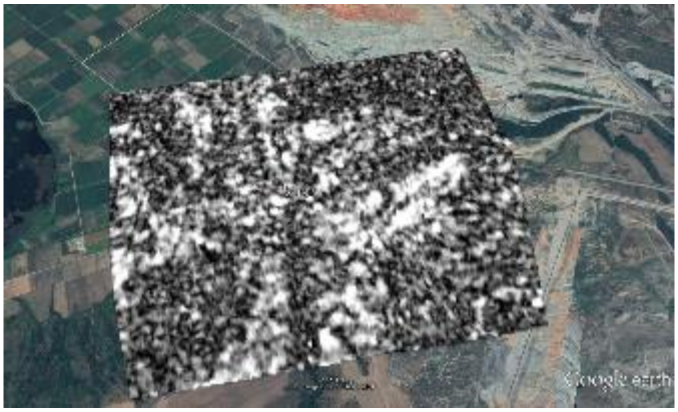

Figure 7.22: From the image, we can see that only a portion of the image has good signal to noise ratio.

Fig (7.23) shows the displacement analysis map of the region. Since the interferogram has low signal to noise ratio, the results from this analysis must not be considered to be accurate.

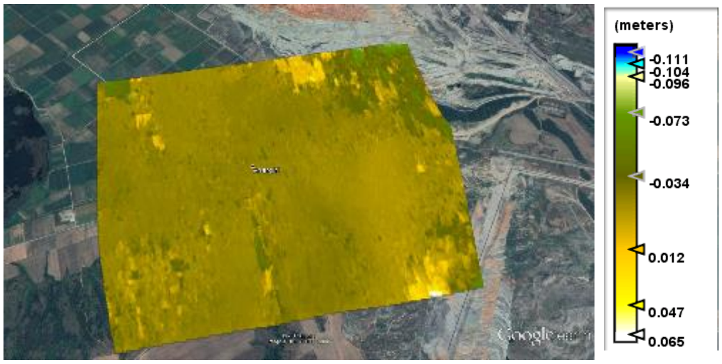

Figure 7.23: The developed displacement map shows that most of area has significant subsidence.

### Test 2

For this test acquisitions taken on May 29,2017 and June 10,2017 are analyzed. The landslide has taken place on June 10,2017

Fig (7.24) Shows the phase of the region. Most of the region is discolored due to high noise. But the highlighted part of image has acceptable coherence and this part shows landslide phase activity.

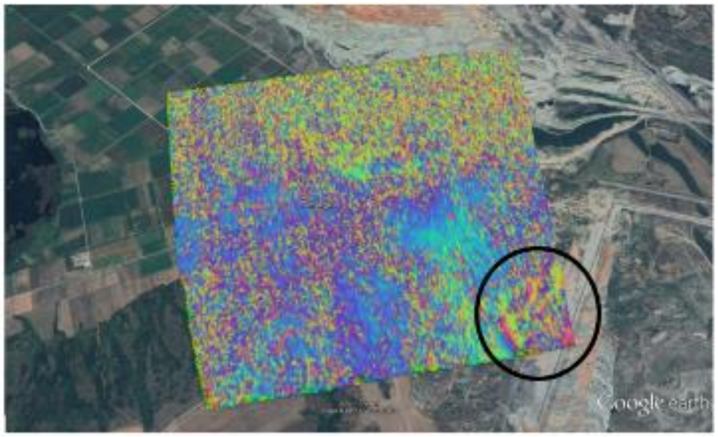

Figure 7.24: Most of the image is discolored due to high noise but the highlighted part shows phase activity corresponding to landslide activity.

Fig (7.25) Shows the coherence map of the region, most the region where the landslide has taken place has poor coherence other than the highlighted area.

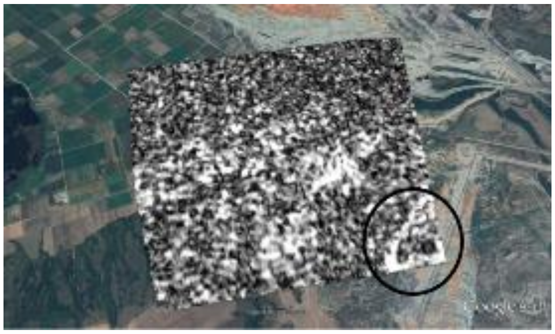

Figure 7.25: The highlighted area contains acceptable coherence and corresponds to landslide activity of the region.

Fig (7.26) shows the displacement analysis map of the region. The highlighted areas are points where landslide has taken place. Region A shows significant subsidence, but this area must not be considered in discussions as the coherence in this region is low and the reading should be considered an abnormality. Region B does not show any significant subsidence related to landslide activity.

Figure 7.26: The figure shows the displacement map of the region. The Region A shows displacement corresponding to landslide activity but must be disregarded due to poor coherence in the area. Region B does not show any subsidence related to landslide activity in the region.

Test 3

For this test acquisitions taken on June 10,2017 and June 22,2017 are analyzed. Landslide has taken place on June 10,2017

Fig (7.27) shows the phase of the region. The phase image is consistently poor for the region and as observed in fig (7.24). The landslide activity in highlighted area in this image is much clear.

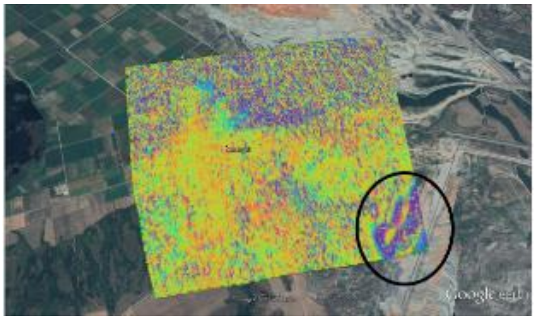

Figure 7.27: In the figure, the highlighted landslide incident is much clear in this image

Fig (7.28) Shows the coherence map of the region, most of the landslide area is under poor coherence other than the highlighted area.

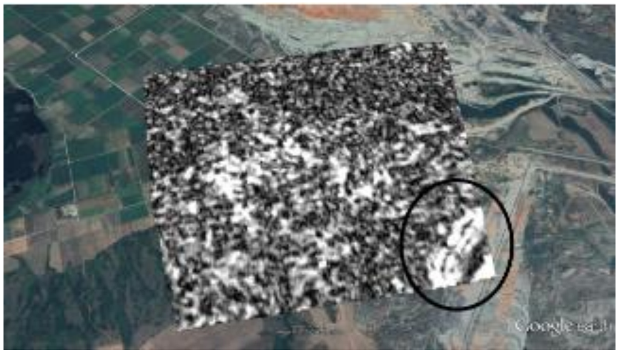

Figure 7.28: In the figure, the highlighted area shows good coherence and corresponds to landslide activity of the region.

Fig (7.29) shows the displacement analysis map of the region. The highlighted area shows significant subsidence. But the area highlighted by A shows has poor coherence and the corresponding subsidence can be considered as abnormality. The area highlighted by B shows subsidence which can be related to the landslide activity in the area.

Figure 7.29: The figure shows the displacement map of the region. Highlighted area A shows significant subsidence but cannot be attributed to the landslide because of poor phase readings. Highlighted area B also shows significant subsidence but because this area has significantly better phase value this subsidence can be attributed to landslide.

### *Discussion*

The coherence in all the 3 tests performed are low resulting in poor phase maps. This could be due to several factors effecting different stages of the interferogram generation process like imaging geometry and high perpendicular baseline. Test 1 shows most of test area has low coherence the resulting phase map is filled with noise making the displacement map not accurate.

The slave image of test 2 was taken on the day after the landslide event. Most of the image has high noise and low coherence the highlighted part of the image has high coherence and is showing fringe which represents landslide activity. In the displacement map the highlighted area A has landslide occurrence but since this region falls in high noise location this part of data cannot be confirmed.

The master image of test 3 was taken on the day after the landslide event. The coherence map shows low coherence throughout the image other than the highlighted area. The phase image also shows lot of noise but the highlighted area representing landslide activity has high coherence. The displacement map from test 3 also shows maximum displacement in the area where landslide has been confirmed to have occurred. But the measured displacement of max 0.65m is not an accurate assessment as can be seen from newspaper reports of the area (Chrysopoulos, 2017).

Overall because of poor signal to noise ratio of the area accurate analysis cannot be performed.

# Chapter 8
# Conclusions and Recommendations

## Conclusion

This work focuses on testing the extent of InSAR technique DInSAR in analyzing different type of landslides and to test if these techniques can be used in landslide recognition. In the case of Etna, we can see how volcano can create slope instabilities. In the case of California highway-1 we can see a possible way to predict a landslide. DInSAR analysis must be repeated in similar landslides as the mudslide in California highway-1 and compare with site investigations to accurately assess the extent of DInSAR analysis and applicability. But we can also see the limitations of DInSAR in the case of Anargyroi, Greece where due to poor coherence we were not able to obtain meaningful results. The displacement analysis is inconclusive because of calibration errors and software limitations. This is also compounded because of dependency on the coherence of the acquisitions.

## Recommendations

From this research, we were able to detect slope movement but could not accurately measure the displacement of the region in two cases where the readings were available.

Additional DInSAR analysis must be performed in different Line of Sight directions (descending) to get accurate estimation of landslide activity and improve the displacement maps. There are some additional complex techniques (PSInSAR) that use time series analysis to negate the effects of poor coherence in some acquisitions. This technique is mentioned in next and future research must be performed in this direction. Although DInSAR analysis was able to detect slope movement and landslide activity it is not able to accurately measure the displacement.

### PSInSAR

Persistent or Permanent Scatterer (PS) InSAR is an advanced DinSAR technique which focuses on identifying coherent target in a stack of images and filter out decorrelation from different entities. This technique has a potential to detect millimeter range variations and can successfully be applied in urban environment.

The technique involves comparing the phase of multiple images and finding persistent scattersers (coherent radar targets). Then using these coherent targets to remove the effect of atmospheric phase components from rest of stack. This also helps to remove errors caused by the ionosphere and orbital components.This principle is used in PSInSAR although the algorithm changed over a period of time the core concept remains the same(Ferretti, Prati, and Rocca 2001)

Although PS technique is more accurate and can remove atmospheric phase most of the time, it has its own disadvantage. To perform this technique, we need 30 InSAR images ideally. This is a huge drawback when the target has limited SAR coverage. Therefore, PSInSAR cannot replace traditional InSAR yet.

### Application of InSAR in Railway.

InSAR technique has been successfully applied in conjugation with HSR (high speed railway) in China, Taiwan and other Asian countries. These techniques have been used to detect instability due to permafrost and ground water abstraction (Fulong Chen, 2012). In Spain DInSAR has been used to monitor sinkhole activity. The test has been conducted on 2 railways stretches. Sinkhole activity was observed in some poorly maintained railroad. From the experiment, the results suggest that DInSAR method can be used to identify and monitor deformations of railways (J. P. Galve, 2015). It was also suggested the test to be coupled with ground based measurements. Application of PSA technique to detect land subsidence over HSR has been found to be highly accurate. High precision was available due to high coherent railway lines which greatly helped in successful application of PSA technique to detect ground subsidence in millimeter range (Yang, 2015).

# References

(n.d.).

A.Corsini, F. A. (2009). Coupling geomorphic field observation and LiDAR derivatives to map complex landslides. *Research Gate*.

A.Walther, B. a. (2008). InSAR processing for the recognition of landslides. *Advances in Geosciences*, 189-194.

Agram, P. S. (2012). *Principles and theory of radar interferometry*. Jet propulsion laboratory.

AIRBUS defence and space. (2014). *Terra SAR-X Image product guide.*

Alessandro Ferretti, A. M.-G. (2007). *InSAR Principles: Guidelines for SAR Interferometry Processing and Interpretation.* ESA Publications.

Alessandro Ferretti, C. P. (2001). Permanent Scatterers in SAR Interferometry. *IEEE TRANSACTIONS ON GEOSCIENCE AND REMOTE SENSING*.

Andre stumpf, j. p. (2017). Correlation of satellite image time-series for the detection and monitoring of slow-moving landslides. *Remote sensing of environment*, 40-55.

Andre Stumpf, N. K. (2011). Object-Oriented Change Detection for Landslide Rapid Mapping. *IEEE Geoscience and Remote Sensing Letters ·*.

array systems. (2017, 06 11). *synthetic analysis tool*. Retrieved from http://www.array.ca/solutions/sar-simulation.html

Blaschke, T. (2009). Object based image analysis for remote sensing. *ISPRS Journal of Photogrammetry and Remote Sensing*.

Brockmann Consult. (2017, 06 11). *SNAP*. Retrieved from http://web.brockmann-consult.de/portfolio/earth-scientific-image-processing/

C. Delacourt, P. A. (2004). Velocity field of the ‘‘La Clapie`re’’ landslide measured by the correlation of aerial and QuickBird satellite images. *GEOPHYSICAL RESEARCH LETTERS*.

Carl, W. (1951). Synthetic Aperture Radars. *IEEE*.

Christophe Delacourt, D. R. (2009). Observation of a Large Landslide on La Reunion Island Using. *sensors*.

Chrysopoulos, P. (2017, 07 10). *Mining-Induced Landslide in Greece Buries €500 Mln Worth of Lignite, Costs 1,700 Jobs*. Retrieved from greece.greekreporter: http://greece.greekreporter.com/2017/06/12/mining-induced-landslide-in-greece-buries-e500-mln-worth-of-lignite-costs-1700-jobs/

Costantini, M. (1998). A Novel Phase Unwrapping Method. *IEEE TRANSACTIONS ON GEOSCIENCE AND REMOTE SENSING*.

CRISP. (2017, 10 28). *Interpreting Optical Remote Sensing Images*. Retrieved from crisp.nus.edu: https://crisp.nus.edu.sg/~research/tutorial/opt_int.htm

Cruden, D. M. (1991). A simple definition of a landslide. *Bulletin of the International Association of Engineering Geology*.

Cruden, V. a. (1996). *landslides : investigation and mitigation chapter 3 landslide types and processes.*

Dario Tarchi, N. C. (2003). Landslide monitoring by using ground-based SAR interferometry:an example of application to the Tessina landslide in Italy. *Engineering Geoglogy*.

E. Brückl, F. B. (2006). Kinematics of a deep-seated landslide derived from photogrammetric, GPS and geophysical data. *Engineering Geology*.

*EM-DAT* . (n.d.). Retrieved from Centre for Research on the Epidemiology of disasters: http://www.emdat.be/

Emerson VieiraMarcelino, A. R. (2009). Landslide inventory using image fusion techniques in Brazil. *International Journal of Applied Earth Observation and Geoinformation*, 181-191.

Ercanoglu, T. A. (2011). Assessment of ASTER satellite images in landslide inventory mapping:Yenice-Go¨kc¸ebey (Western Black Sea Region, Turkey). *Bull Eng Geol Environ*.

ESA. (2016, 12 15). *sentinel-1 overview*. Retrieved from earth esa user guide: https://earth.esa.int/web/sentinel/user-guides/sentinel-1-sar/overview

ESA. (2017, 09 18). *Level-1 interferometric wide swath SLC products*. Retrieved from ESA sentinel-1 technical guide: https://earth.esa.int/web/sentinel/interferometric-wide-swath-slc

ESA. (2017, 04 10). *naming conventions*. Retrieved from earth esa: https://earth.esa.int/web/sentinel/user-guides/sentinel-1-sar/naming-conventions

F.Guzzettia, F. M. (2011). Seasonal landslide mapping and estimation of landslide mobilization rates using aerial and satellite images. *Geomorphology*, 59-70.

Fausto G, M. M. (2009). Analysis of Ground Deformation Detected Using the SBAS-DInSAR. *Pure and Applied Geophysics*.

Fausto Guzzettia, ∗. A.-T. (2011). landslide inventory maps :new tools to old problems. *earth science review*.

Ferretti, A. (2014). *Satellite InSAR Data Reservoir Monitoring from space.* EAGE.

Franny Giselle Murillo-García, I. A.-A. (2013). Satellite stereoscopic pair images of very high resolution:. *Springer-Verlag Berlin Heidelberg 2014*.

Fulong Chen, H. L. (2012). Interaction between permafrost and infrastructure along the Qinghai–Tibet Railway detected via jointly analysis of C- and L-band small baseline SAR interferometry. *Remote sensing of Environment*, 532-540.

G.Bitelli, M. A. (2003). *Terrestrial laser scanning and digital photogrammetry techniques to monitor landslide bodies.* University of Bologna.

Gillespie, A. K. (1987). Color enhancement of highly correlated images—channel ratio and ‘chromaticity’ transformation techniques. *Remote Sensing of Environment*, 343-365.

GIM International. (2017, 10 11). *satellite radar interferometry*. Retrieved from GIM international: https://www.gim-international.com/content/article/satellite-radar-interferometry

GISGeography. (2017, 10 31). *A complete guide to LiDAR:light detection and Ranging*. Retrieved from gisgeography: http://gisgeography.com/lidar-light-detection-and-ranging/

Goldstein, R. M. (1998). Radar interferogram filtering for geophysical applications. *Geophysical Research Letters*.

Guarnieri, F. D. (2006). TOPSAR: Terrain Observation by Progressive Scans. *IEEE Transactions on Geoscience and Remote Sensing*, 2352-2360.

H.Cornforth, D. (2005). *Landslide in practice.* john wiley & sons.

Hanssen, R. F. (2001). *Radar Interferometry – Data Interpretation and Error Analysis.* Kluwer Academic Publishers.

Hindustan times. (2013, june 19). *Kedarnath temple stays intact, its surroundings have gone with flow*. Retrieved from hindustan times: http://www.hindustantimes.com/india/kedarnath-temple-stays-intact-its-surroundings-have-gone-with-flow/story-usmJ2UmB9Rc8ZQCrLTR4kN.html

IAEG. (1990). Suggested nomenclature for landslides. *Bulletin of the International Association of Engineering Geology - Bulletin de l'Association Internationale de Géologie de l'Ingénieur*, 13-16.

J, M. D. (2008). *Imaging with Synthetic Aperture Radar.* EPFL.

J. M. Duncan, R. W. (1986). *the report of the Thistle Slide Committee to state of Utah.* denver: U.S geological survey.

J. P. Galve, C. a. (2015). Railway deformation detected by DInSAR over active sinkholes in the Ebro Valley evaporite karst, Spain. *Natural Hazards and Earth System Science*.

Leonardo Cascini, G. F. (2009). A new approach to the use of DINSAR data to study slow moving landslides over large areas.

Liu, J. (2000). Smoothing filter based intensity modulation: a spectral preserve image fusion technique for improving spatial details. *International Journal of Remote Sensing*, 3461–3472.

Marco Scaioni, L. L. (2014). Remote Sensing for Landslide Investigations: An Overview of Recent Achievements and Perspectives. *remote sensing*.

Massonnet, D. &. (1990). Synthetic Aperture Radar : New Processing Concepts. *IGARSS*.

Mathew, P. (1999). *Computer Processing of Remotely Sensed Images.* New York: John Wiley and Sons.

Michel Jaboyedoff, T. O.-H. (2010). Use of LIDAR in landslide investigations: a review. *Nat Hazards*.

Mio Kasai, M. I. (2009). LiDAR-derived DEM evaluation of deep-seated landslides in a steep and rocky region. *Geomorphology*, 57-69.

Monique Moine, A. P.-P. (2009). Detection of landslides from aerial and satellite images with a semi-automatic method. Application to the Barcelonnette basin. *Landslide processes - from geomorphologic mapping to dynamic*, 63-68.

Munzer, j. a. (2010). Automatic archaeological feature extraction from satellite VHR images. *ACT Astronautica*, 1302-1310.

Nair, A. (2014). *Understanding the Causes of Uttarakhand Disaster of June 2013: A Scientific Review*. Trivandrum.

O. Monserrat, M. ,. (2014). A review of ground-based SAR interferometry for deformation measurement. *ISPRS Journal of Photogrammetry and Remote Sensing*.

Pamela, E. C. (2009). *Remote Sensing Tools for Exploration.* Springer.

Paolo M, F. B. (2015). Terrestrial SAR Interferometry Monitoring of Natural slopes and Man made structures. , *Engineering Geology for Society and Territory*.

Pascal Lacroix, B. Z. (2013). Supervised Method of Landslide Inventory Using Panchromatic SPOT5 Images and Application to the Earthquake-Triggered Landslides of Pisco (Peru, 2007, Mw8.0). *Remote Sensing for Landslides Investigation: From Research into Practice*.

Richards, J. (2009). *Remote Sensing with Imaging Radar.* Springer.

Silvia Bianchini, G. H. (2013). Landslide Activity Maps Generation by means of persistent scatterer Interferometry. *Remote Sensing*.

Snyder, G. F. (2009). Monitoring slope movements. *The Geological Society of America*.

terzaghi. (1950). *Mechanism of Landslides. In Engineering Geology (Berkel)* . The Geological Society of America.

The Canadian Geotechnical Society. (1993). *Multilingual Landslide Glossary*. Richmond : Bi Tech Publishers Ltd.

Tomas M.Lillesan, R. W. (2004). *remote sensing and image interpretation.* john wiley and sons.

Tomas M.Lillesand, R. W. (2004). *Remote Sensing and Image Interpretation.* John Wiley & Sons.

Travelletti J., D. C.-P. (2011). *Correlation of multi-temporal ground-based images for landslide monitoring: application, potential and limitations.*

UNAVCO. (2015, August 15). *synthetic aperture radar satellites*. Retrieved from UNAVCO.org: https://www.unavco.org/instrumentation/geophysical/imaging/sar-satellites/sar-satellites.html

USGS . (2006). *Landslide types and processes.*

Veci, L. (2016). *TOPS Interferometry Tutorial.* ESA.

Weitao Chen, X. L. (2014). Forested landslide detection using LiDAR data and the random forest. *remote sensing of environment*.

Weng, Q. (2009). Thermal infrared remote sensing for urban climate and environmental studies: Methods, applications and trends. *ISPRS Journal of Photogrammetry and Remote Sensing*, 335-344.

Wong, J. a. (2005). satellite remote sensing for detailed landslide inventories using change detection and image fusion. *international journal of remote sensing*.

Y.Haeberlin, P. T. (2005). VALIDATION OF SPOT-5 SATELLITE IMAGERY FOR GEOLOGICAL HAZARD IDENTIFICATION AND RISK ASSESSMENT FOR LANDSLIDES, MUD AND DEBRIS FLOWS IN MATAGALPA, NICARAGUA.

Yang, Z. (2015). *Monitoring and Predicting Railway Subsidence Using InSAR and Time Series Prediction Techniques.* Birmingham: The University of Birmingham.

Zhang, Y. (2002). Problems in the fusion of commercial high-resolution satellite as well as Landsat 7 images and initial solutions. *Proceedings of Symposium on Geospatial Theory, Processing and Applications of ISPRS.* ottawa.

# Appendix A

# List of Definitions

### TOPSAR

TOPSAR is Terrain Observation with Progressive Scans SAR is an acquisition technique. Where data is acquired in long burst by scanning continuously throughout the acquisition from backward to forward. This technique is superior to ScanSAR because this technique is capable of generating homogeneous image quality and same signal-to-noise ratio throughout the swath. This technique causes worsening of azimuth resolution as it concentrates on range coverage to resolution (Guarnieri, 2006).

### Coregistration

Coregistration is critical step in which the SAR images from two different acquisitions are aligned. This step is needed to accurately measure phase difference and to reduce noise in the image.

### Computation of Interferogram

The process of creating an Interferogram involves the subtraction of flat-earth phase. Flat-earth phase is estimated using the orbital and metadata information. The flat-earth phase is the phase present in the signal (P) due to curvature of reference surface.

### TOPS Deburst

Each sub-swath in the acquisition consists of number of bursts. Each burst behaves like a separate SLC (Single look Complex) image. These bursts are separated by demarcation zones that may contain garbage values. The process of removing these demarcation zones and making all burst data in to single product is called Debursting.

### TOPS Merging

Each acquisition consists of 3-5 sub-swath based on type of product (3 for IW and 5 for EW). When processing, the sub-swath is chosen depending on target area. Sometimes the target area can lie in between 2 sub-swaths. The process of merging these two sub-swaths to obtain a single product for further analysis is called TOPS Merging

### Goldstein Phase Filtering

The quality of the interferogram map is improved by filtering noise. The Goldstein phase filtering method is used to improve the sharpness of the image before the phase unwrapping stage to improve the results in the phase unwrapping process.

### Phase Unwrapping

Phase unwrapping is the process of recovering absolute phase data from an array of phase values known only modulo 2 rad. This process is performed in SNAPHU which produces completely unwrapped results which can be used for deformation analysis.

### SRTM

Shuttle Radar Topography Mission are DEM developed by radar systems on board the space shuttle Endeavour. This type of DEM is used as reference DEM models for DInSAR analysis. They have been released to public on September 23,2014 by United States Government.

MCF

Minimum Cost Flow Algorithm is a phase unwrapping technique better explained in (Costantini, 1998)

Range Doppler Correction

Range Doppler Terrain Correction is an orthorectification method for geocoding SAR images. It uses available orbit state vector information from metadata and other parameters like radar timing annotations with reference to DEM data to derive precise geolocation information.

Perpendicular Baseline

The distance between two acquisition spots perpendicular to the satellite viewing direction is known as the ‘perpendicular baseline’. The smaller the perpendicular baseline the accurate the analysis is going to be (GIM International, 2017).

Polarization.

Polarization corresponds to the direction in which radar waves are transmitted and received. Depending on the polarization the results of the experiment can change significantly. Sentinel-1 has 4 level of polarization complexity i.e. it can transmit and receive signals in all polarizations.

DEM

Digital Elevation Model is a digital representation of the terrain surface in 3-D.